PHYSICAL REVIEW B **79**, 045321 (2009)

Effects of disorder in three-dimensional Z_2 quantum spin Hall systems

Ryuichi Shindou[1] and Shuichi Murakami[2,3]
[1]*Furusaki Condensed Matter Theory Laboratory, RIKEN, 2-1 Hirosawa, Wako, Saitama 351-0198, Japan*
[2]*Department of Physics, Tokyo Institute of Technology, 2-12-1 Ookayama, Meguro-ku, Tokyo 152-8551, Japan*
[3]*PRESTO, Japan Science and Technology Agency (JST), Kawaguchi, Saitama 332-0012, Japan*
(Received 8 August 2008; revised manuscript received 31 December 2008; published 30 January 2009)

In this paper, we address ourselves to the nonmagnetic disorder effects onto the quantum critical point, which intervenes the three-dimensional Z_2 quantum spin Hall insulator (topological insulator) and an ordinary insulator. The minimal model describing this type of the quantum critical point is the single copy of the 3 +1 Dirac fermion, whose topological mass m induces the phase transition between the topological insulator and an ordinary one. We first derive the phase diagram spanned by the mass term m, chemical potential μ, and strength of the disorder within the self-consistent Born approximation. By way of this, we find a finite density of state appears even at zero energy and at the phase-transition point, i.e., $m=\mu=0$, if the strength of the disorder potential exceeds some critical value. To infer the structure of the low-energy effective theory around these zero-energy states, we further calculated the weak-localization correction to the conductivity. To be more specific, we have found that the diffuson is dominated by the charge diffusion mode and parity diffusion mode. While the charge diffusion mode always carries the diffusion pole, the parity diffusion mode becomes massless only at $m=0$, but suffers from the infrared cutoff for nonzero m. Corresponding to this feature of the diffuson, the Cooperon is also composed of two quasidegenerate contributions. We found that these two give rise to the same magnitude of the anti-weak-localization (AWL) correction with each other at $m=0$. As a result, when the topological mass m is fine tuned to be zero (but for generic μ), the AWL correction becomes doubled (quantum correction doubling). Based on this observation, we will discuss the possible microscopic picture of the "levitation and pair-annihilation" phenomena, recently discovered by Onoda *et al.* [Phys. Rev. Lett. **98**, 076802 (2007)].

DOI: 10.1103/PhysRevB.79.045321 PACS number(s): 73.20.Fz, 73.43.−f, 85.75.−d

I. INTRODUCTION

Physics of spin transport has been a matter of intensive research in recent years. One of the topics of current interest is the spin Hall effect. This has been originally proposed theoretically[1,2] and later followed by various experimental results.[3,4] The research on the spin Hall effect opens a new field of Hall effects in time-reversal invariant systems. This has also led us to a new concept of the quantum spin Hall effect, which is the natural "spin" extension of the quantum Hall effect.[5–7] In the quantum spin Hall effect in two dimensions, the bulk is gapped while there are gapless edge states carrying spin current. In this case, the external magnetic field is zero, while the spin-orbit coupling acts as a "spin-dependent magnetic field," giving rise to the effect analogous to the quantum Hall effect. Such insulators showing the quantum spin Hall effect are characterized by the Z_2 topological number.[5] We shall call them as Z_2 quantum spin Hall insulators (QSHI).

The simplest system for the two-dimensional (2D) Z_2 QSHI is realized as a superposition of the wave functions of two quantum Hall subsystems,[5–7] one with spin up and the other with spin down, having opposite Chern numbers. The system respects not only the time-reversal ($\mathcal{T}$) invariance but also the spin conservation. Such an insulator supports the same numbers of right-moving up-spin edge states and left-moving down-spin edges.

This Kramers pair of chiral edge states is often called as the helical edge state. By its construction, the number of this Kramers pairs of edge states corresponds to the Chern integer associated with its bulk-wave function.[8] The $\mathcal{T}$ symmetry guarantees the double degeneracy between right-moving up-spin and left-moving down-spin states. Thus, the stability of *each* Kramers pair is supported by this $\mathcal{T}$ symmetry.

Spin nonconserving (but $\mathcal{T}$ invariant) perturbations, however, introduce level repulsions between two *different* Kramers pairs. Namely, they usually let two pairs annihilate with each other, and open a gap. Accordingly, in the presence of generic spin-nonconserving perturbations, those wave functions having *even* numbers of Kramers pairs reduce to *trivial* insulators, which have no gapless edge states.[9–12] Meanwhile, wave functions having *odd* numbers of pairs still can have one active helical edge mode. The latter is dubbed as the Z_2 quantum spin Hall (topological) insulator. Thus, stability of such a gapless edge state is protected only by the $\mathcal{T}$ symmetry, which does not require spin-conservations anymore.[9–14]

The three-dimensional (3D) version[15–20] of the Z_2 QSHI carries same characters as that of 2D does. The 3D Z_2 QSHI also allows any spin-nonconserving perturbations, while always requires the $\mathcal{T}$ symmetry. Simultaneously, however, it is not a mere extension of the 2D Z_2 QSHI, in a sense that 3D Z_2 QSHI has *no* $U(1)$ analog of QSHI. Namely, they support a 2+1 massless Dirac fermion as its surface state,[15,19] instead of a helical edge state. In the 2D surface Brillouin zone, say k_x-k_y plane, this massless Dirac fermion has a spin which depends on the (surface) crystal momentum. It is clear that such an insulator cannot be adiabatically connected into a composite of two spinless wave functions. In such Z_2 QSHI,

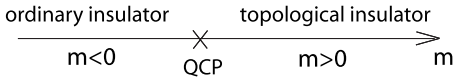

FIG. 1. A schematic phase diagram for the quantum critical point intervening the Z_2 QSHI and an ordinary insulator. m is a system parameter driving the phase transition. When $m=0$, the system is in a critical phase. In the Fu-Kane-Mele model, it corresponds to the relative strength of one out of the four nearest neighbor transfer integrals emitting from a single diamond lattice site.

the $\mathcal{T}$ symmetry therefore guarantees the massless nature of each 2+1 surface Dirac fermion.

Z_2 QSHI always has a quantum critical point (QCP) at its phase boundary to any ordinary insulators, in both 2D and 3D. For example, from the 3D tight-binding model proposed by Fu *et. al.*,[15] we can explicitly see this; when a certain $\mathcal{T}$ symmetric parameter is varied in their model, 3D Z_2 QSHI is driven into an ordinary insulator, latter of which does not support any surface states (see Fig. 1). Observing this, a following question naturally arises; during this tuning, the $\mathcal{T}$ symmetry is *always* preserved so that the massless nature of the surface Dirac fermion is supposed to be protected by this. At the same time, however, this 2+1 surface fermion should have become "massive" when a system enters an ordinary insulator phase. Thus, one might ask how this single surface Dirac fermion could acquire a finite mass, with keeping the $\mathcal{T}$ symmetry.

The answer is simple; we have *two* sample boundaries, say $z=+L$ and $z=-L$. Each boundary supports one 2+1 surface massless Dirac fermion. They are localized at each boundary, when the bulk gap is sufficiently large. In such a situation, a mixing between these two 2+1 surface massless Dirac fermions is tiny, i.e., $\mathcal{O}(e^{-L/\xi})$ with ξ being the localization length. However, when a system becomes close to the quantum critical point, a mixing between these two surface states becomes substantial with increasing ξ. When a bulk eventually reaches the quantum critical point, two surface massless Dirac fermions readily communicate via extended bulk states. Thus, they generally annihilate in pairs, just as in those insulators having even number of 2+1 surface Dirac fermions at one boundary.

This simple picture in the clean limit raises the following nontrivial speculations about the disorder effects on the Z_2 QSHI. Suppose that $\mathcal{T}$-symmetric random potentials are introduced in the topological insulator phase. When the corresponding bulk gap is sufficiently large, we could begin with two separate bands. The scaling argument in 3D (Ref. 21) tells us that each band should always have two mobility edges, respectively [see Fig. 2(b)]. Namely, there is no delocalized bulk-wave function near the zero energy. Starting from this phase, let us change some $\mathcal{T}$-invariant model parameters so that a bulk transits from this topological insulator to an ordinary one. From the argument in the clean limit, one can then expect that *a delocalized bulk-wave function should emerge at the zero-energy region at the quantum critical point*, i.e., $\mu=m=0$ [see Fig. 2(a)]. If it were not, the two surface states localized at the two sample boundaries could not communicate at all and they could not annihilate with each other. As a result, the system was unable to smoothly

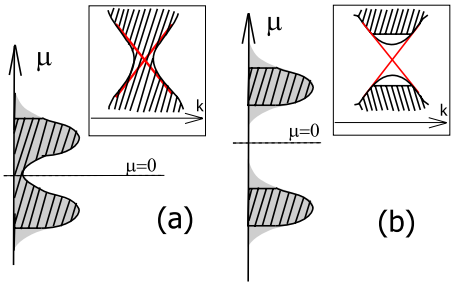

FIG. 2. (Color online) A schematic picture of the density of state and mobility edges, where hatched region corresponds to the extended state. Inset represents the energy dispersion as a function of surface crystal momentum, where the two crossing lines (red lines) correspond to the surface state at $z=\pm L$. (a) $m=0$; at quantum critical point. (b) $m>0$; in the topological insulator phase.

enter an ordinary band insulator since the latter one does not support any surface state at all.

To put this reversely, the existence of the QCP having extended bulk-wave functions is always required, whenever this critical point separates an ordinary insulator and the topological insulator. This is because these two insulating phases support different numbers of Kramers pairs of surface states. Moreover, provided that each surface state is stable by itself, this QCP should be also stable *however small* the density of state (DOS) at the zero energy is and *however strong* the disorder strength is. Otherwise, the topological insulator could be adiabatically connected into an ordinary band insulator, which contradicts the different Z_2 topological numbers for the two phases.

In this paper, we will uncover several intriguing features associated with the nonmagnetic disorder effects onto this topological quantum critical point. The organization of this paper is summarized as follows. In Sec. II, we will briefly review the effective continuum model for the quantum critical point intervening the Z_2 topological insulator and an ordinary insulator. The effective model is known to be described by the 3+1 Dirac fermion, whose mass term brings about the topological quantum phase transition. Namely, when the mass term changed from positive to negative, a system transits from the topological insulator to an ordinary insulator. As such, we call this mass term especially as the topological mass term. Based on this effective model, we will next introduce various types of the on-site random potentials respecting the $\mathcal{T}$ symmetry. Note that, in this paper, we restrict ourselves to $\mathcal{T}$-symmetric cases and exclude magnetic impurities because, in the absence of the $\mathcal{T}$ symmetry, the two phases are no longer topologically distinct.

Based on the self-consistent Born approximation, we first work over the single-particle Green's function in Sec. III. The phase diagram spanned by the (bare) chemical potential μ, (bare) mass term m, and strength of the disorder α is derived. In particular, at the critical point, i.e., $m=0$, we found some critical value of the disorder strength, α_c, above which the zero-energy state, i.e., $\mu=0$, acquires a finite lifetime τ,

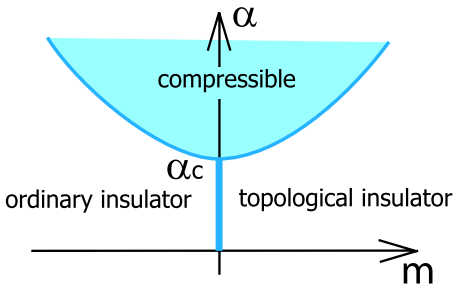

FIG. 3. (Color online) A schematic phase diagram for $\mu=0$. A blue shaded region corresponds to a compressible phase, which separates two gapped phases, i.e., an ordinary insulator and the topological insulator. The phase boundary for $\alpha>\alpha_c$ is given by $1-\frac{\alpha_c}{\alpha}\equiv\frac{m}{2}\arctan[\frac{2}{m}]$.

$$\frac{1}{\tau}\arctan[\tau]=1-\frac{\alpha_c}{\alpha}. \tag{1}$$

Since the density of state in our model is always proportional to the inverse of the lifetime (see below), nonzero τ^{-1} simply means that a system is in a compressible phase.

When a finite but small topological mass m is introduced for $\alpha>\alpha_c$, the lifetime τ and the renormalized mass $\bar{m}$ becomes as follows:

$$\left(\frac{1}{\tau},\bar{m}\right)=\left(\sqrt{\frac{1}{\tau_0^2}-\frac{m^2}{4}},\frac{m}{2}\right), \tag{2}$$

where τ_0 is given as a function only of α via Eq. (1). Thus, when the bare topological mass exceeds the critical value $m_c\equiv 2\tau_0^{-1}$, the density of state vanishes so that a system enters an incompressible phase. This gapped phase can be adiabatically connected into band insulator phases in the clean limit. Accordingly, we will reach the phase diagram for the zero-energy state as depicted in Fig. 3. In Sec. III, we also describe the behavior of the one-particle Green's function for a finite μ (see below), in which we observe that the compressible phase (not necessarily metallic phase) always intervenes the topological insulator phase and an ordinary insulator phase as in Fig. 3.

Focusing on this intervening compressible phase, especially for $\alpha<\alpha_c$, we will derive in Sec. IV the diffuson, Cooperon, and the weak-localization correction to the electric conductivity. We will first observe that the diffuson is composed of two quasidegenerate low-energy modes,

$$\hat{\Gamma}^d(q,\omega)\propto\frac{1}{\omega+iDq^2}\hat{\Gamma}_1^d+\frac{1}{\omega+iDq^2+i\tau_{\text{topo}}^{-1}}\hat{\Gamma}_2^d+\cdots \tag{3}$$

[see Fig. 11 or Eq. (74) for the definition of $\hat{\Gamma}^d(q,\omega)$]. The first term participates in usual charge diffusion mode, and therefore always has the diffusion pole, i.e., $[\omega+iDq^2]^{-1}$ (ω and q stand for the frequency and momentum of the density fluctuation, respectively). The other low-energy mode, however, becomes massless only in the absence of the topological mass m. Namely, its low-energy and long-wavelength behavior is generally truncated by the infrared cutoff τ_{topo}^{-1}, while this infrared cutoff reduces to zero at $m=0$ (but generic μ), i.e., $\tau_{\text{topo}}^{-1}\propto m^2$.

Physically speaking, this second mode describes the diffusion of the parity-density degree of freedom, which becomes a conserved quantity of our effective Hamiltonian at $m=0$. Namely, the parity-density correlation function exhibits the diffusion pole structure at the critical point ($m=0$), while it becomes massive in the presence of the finite topological mass. Consequently, the diffuson acquires one additional low-energy, i.e., the second term of Eq. (3), into which the information of this parity-density correlation function is separately encoded.

When the hole line of the diffuson time reversed, these two-mode features are transcribed into the Cooperon: the Cooperon thus obtained is also composed of two quasidegenerate dominant contributions,

$$\hat{U}^{\text{coop}}(k+k',\omega)\propto\frac{1}{\omega+iD(k+k')^2}\hat{U}_1^c+\frac{1}{\omega+iD(k+k')^2+i\tau_{\text{topo}}^{-1}}\hat{U}_2^c+\cdots \tag{4}$$

[see Fig. 11 and its caption for the definition of $\hat{U}^{\text{coop}}(k+k',\omega)$]. In Sec. IV, we will see that, at the critical point ($m=0$), these two contributions give rise to the same amplitude of the anti-weak-localization (AWL) correction to the electric conductivity. When the finite topological mass is introduced, however, the Cooperon associated with the parity mode channel becomes ineffective since its backward-scattering behavior is truncated by the cutoff τ_{topo}^{-1}. Meanwhile, the Cooperon obtained from the charge mode channel remains effective even in the presence of finite m. As a result, the AWL correction at the critical point becomes precisely halved, on introducing the finite topological mass (quantum correction doubling).

In terms of this behavior of the parity diffusion mode and that of the corresponding AWL correction, we will argue in Sec. V the possible microscopic mechanism of how the delocalized bulk-wave function emerges at the critical point, i.e., $m=\mu=0$. To be more specific, we expect that the parity diffusion mode mentioned above generally becomes massless, when a system transits from the topological insulator side to the ordinary insulator side. Assuming that this is the case, we will attribute the emergence of the extended bulk-wave function to the AWL correction obtained from this parity mode channel, i.e., the second term of Eq. (4). For the systematic understanding, however, one generally needs to go beyond the theoretical approach employed in this paper. Several open issues will be also discussed in Sec. V.

A number of appendixes describe other topics useful in understanding the main text in more detail. For clarity of the explanation, we have presented the results only in the case of chemical-potential-type disorder in the text. The study in the presence of general $\mathcal{T}$-symmetric disorders becomes more cumbersome. But the basic feature such as the phase diagram is expected to be same. In Appendix A, we will describe how the one-particle Green's function at the zero-energy state behaves in the presence of these general $\mathcal{T}$-invariant random potentials.

Our weak-localization calculation described in Sec. IV is the controlled analysis, when it comes to the weakly disordered region, $\alpha < \alpha_c$. Namely, for this parameter region, one can confirm self-consistently the coupling constant $1/k_F l \equiv 1/\mu\tau$ to be sufficiently small around $\mu=0$ [see Eq. (70)]. For $\alpha > \alpha_c$, however, this coupling constant generally diverges toward $\mu=0$, only to make the weak-localization calculation [and self-consistent Born (scB) calculation] an uncontrolled analysis. Thus, as the complementary analysis for this strongly disordered region, $\alpha > \alpha_c$, we employed the mode-mode coupling analysis in Appendixes B–D. By taking into account the quantum interference effect due to the Cooperon terms, this theoretical framework gives us the gap equation for the diffusion constant. Main results in Sec. IV such as the quantum correction doubling are also supported by the analysis in Appendixes B–D.

II. EFFECTIVE CONTINUUM MODEL AND DISORDER

A. Effective continuum model

We consider a system with both $\mathcal{T}$ symmetry and the spatial inversion ($\mathcal{I}$) symmetry. Under this symmetry requirement, Murakami *et al.*[22,23] recently derived the minimal model for an arbitrary quantum critical point intervening the topological insulator and an ordinary insulator on a quite general ground. It turns out to be always described by the 3+1 Dirac fermion given as follows:

$$\mathcal{H}_0 \equiv \int d^3 r \psi^\dagger(r) \left\{ \sum_{\mu=1}^{3} \hat{\gamma}_\mu (-i\partial_\mu) - m\hat{\gamma}_5 \right\} \psi(r), \tag{5}$$

where m corresponds to the topological mass term. Without loss of generality, one can regard the topological insulator phase to be $m>0$ and an ordinary insulator phase to be $m<0$ (see Fig. 1). To see that "m" actually endows this Dirac fermion with a mass, we note that following five 4×4 γ matrices are anticommuting with one another:

$$\hat{\gamma}_1 \equiv \hat{\sigma}_y \otimes 1, \hat{\gamma}_2 \equiv \hat{\sigma}_z \otimes \hat{s}_x, \hat{\gamma}_3 \equiv \hat{\sigma}_z \otimes \hat{s}_y,$$

$$\hat{\gamma}_4 \equiv \hat{\sigma}_z \otimes \hat{s}_z, \hat{\gamma}_5 \equiv \hat{\sigma}_x \otimes 1.$$

The matrices $\hat{\sigma}_\mu$ and $\hat{s}_\mu$ are Pauli matrices, representing the (generalized) sublattice index, and the spin index, respectively. In terms of these Pauli matrices, we will take the $\mathcal{T}$ operator as $i\hat{s}_y K$ with K being the complex conjugation. Meanwhile, the $\mathcal{I}$ operator will be taken as $\hat{\sigma}_x$. It follows from these conventions that $\hat{\gamma}_{1,2,3,4}$ are $\mathcal{T}$ odd and $\mathcal{I}$ odd, while $\hat{\gamma}_5$ is $\mathcal{T}$ even and $\mathcal{I}$ even (see Table I). Together with the property that $-i\partial_\mu$ is $\mathcal{T}$ odd and $\mathcal{I}$ odd, we can easily see that our Hamiltonian in the clean case is indeed $\mathcal{T}$ even and $\mathcal{I}$ even. This guarantees the Kramers degeneracy at each k point, irrespectively of the topological mass m. We also note that Eq. (5) is indeed the low-energy effective continuum Hamiltonian for various lattice models recently discussed in literature.[15,19,24]

Generally speaking, we can enumerate all Hermite matrices possible in this spin-sublattice space. Namely, using the commutator between these five Dirac matrices, we have other $10 \equiv {}_5C_2$ associated Dirac matrices,

TABLE I. Dirac operators and their symmetries.

Dirac matrices	$\mathcal{T}$	$\mathcal{I}$
$\hat{\gamma}_0 \equiv 1 \otimes 1$	+	+
$\hat{\gamma}_1 \equiv \hat{\sigma}_y \otimes 1$	−	−
$\hat{\gamma}_2 \equiv \hat{\sigma}_z \otimes \hat{s}_x$	−	−
$\hat{\gamma}_3 \equiv \hat{\sigma}_z \otimes \hat{s}_y$	−	−
$\hat{\gamma}_4 \equiv \hat{\sigma}_z \otimes \hat{s}_z$	−	−
$\hat{\gamma}_5 \equiv \hat{\sigma}_x \otimes 1$	+	+

$$\hat{\gamma}_{ij} \equiv \frac{1}{2i}[\hat{\gamma}_i, \hat{\gamma}_j] = -i\hat{\gamma}_i\hat{\gamma}_j. \tag{6}$$

We can further classify these ten matrices into two classes; one is $\mathcal{T}$ invariant (even) matrices and the other is $\mathcal{T}$ odd. Since the five Dirac matrices are always even under $\mathcal{I}\cdot\mathcal{T}$, these ten associated Dirac matrices are by construction odd under $\mathcal{I}\cdot\mathcal{T}$. Thus the symmetries of these ten matrices can be summarized as in Table II.

Let us introduce $\mathcal{T}$-symmetric "on-site-type" random potentials as generally as possible,

$$\mathcal{H}_{\text{imp}} \equiv \int dr \psi^\dagger(r) \left\{ v_0 \hat{\gamma}_0 + v_5 \hat{\gamma}_5 + \sum_{j=1}^{4} v_{j5} \hat{\gamma}_{j5} \right\} \psi(r), \tag{7}$$

where all the six components of the vector $\vec{v}(r)$ are real-valued functions of r. Then, each single-particle eigenstate of $\mathcal{H}_0 + \mathcal{H}_{\text{imp}}$ always has a Kramers pair state

$$\langle \tilde{\phi}(r)| \equiv \hat{1} \otimes (-i)\hat{s}_y |\phi(r)\rangle. \tag{8}$$

Namely, $|\tilde{\phi}(r)\rangle$ and $|\phi(r)\rangle$ are degenerate and orthogonal to each other. Noting this, one can see that the retarded (advanced) Green's function observes the following relation in each ensemble:

$$\hat{G}^{R(A)}(r,r';\mu) \equiv \sum_n \frac{|\phi_n(r)\rangle\langle\phi_n(r')|}{\mu - \epsilon_n \pm i\delta}$$

$$= \hat{1} \otimes \hat{s}_y \cdot \{\hat{G}^{R(A)}(r',r;\mu)\}^t \cdot \hat{1} \otimes \hat{s}_y. \tag{9}$$

TABLE II. Dirac associated operators and their symmetries

10 matrices	$\mathcal{T}$	$\mathcal{I}$
$\hat{\gamma}_{15} \equiv -\hat{\sigma}_z \otimes 1$	+	−
$\hat{\gamma}_{25} \equiv \hat{\sigma}_y \otimes \hat{s}_x$	+	−
$\hat{\gamma}_{35} \equiv \hat{\sigma}_y \otimes \hat{s}_y$	+	−
$\hat{\gamma}_{45} \equiv \hat{\sigma}_y \otimes \hat{s}_z$	+	−
$\hat{\gamma}_{12} \equiv \hat{\sigma}_x \otimes \hat{s}_x$	−	+
$\hat{\gamma}_{13} \equiv \hat{\sigma}_x \otimes \hat{s}_y$	−	+
$\hat{\gamma}_{14} \equiv \hat{\sigma}_x \otimes \hat{s}_z$	−	+
$\hat{\gamma}_{23} \equiv 1 \otimes \hat{s}_x$	−	+
$\hat{\gamma}_{34} \equiv 1 \otimes \hat{s}_y$	−	+
$\hat{\gamma}_{42} \equiv 1 \otimes \hat{s}_z$	−	+

B. Disorder averages, spatial inversion symmetry, rotational symmetry, and engineering dimension

As usual, we will take the quenched average of these $\mathcal{T}$ invariant impurities at the Gaussian level,

$$\bar{\cdots} \equiv \frac{1}{\mathcal{N}} \int \mathcal{D}[v] e^{P[v]} \cdots , \tag{10}$$

$$P[v] \equiv \sum_{j,m \in \{0,5,15,\cdots,45\}} \int \int d^3 r d^3 r' [\hat{\Delta}^{-1}]_{(r,j|r',m)} v_j(r) v_m(r'), \tag{11}$$

with a proper normalization factor $\mathcal{N}$ and real-valued symmetric matrix $\hat{\Delta}$. For simplicity, an on-site-type correlation will be assumed,

$$\Delta(r,j|r',m) \equiv \Delta_{jm} \delta^3(r-r'). \tag{12}$$

We also suppose that the translation symmetry and the spatial inversion symmetry are recovered *after* these quenched averages,

$$\hat{G}^{R(A)}(r,r';\mu) \equiv \hat{G}^{R(A)}(r+b,r'+b;\mu), \tag{13}$$

$$\hat{G}^{R(A)}(r,r';\mu) \equiv \hat{\sigma}_x \otimes \hat{1} \cdot \hat{G}^{R(A)}(-r,-r';\mu) \cdot \hat{\sigma}_x \otimes \hat{1}. \tag{14}$$

Then, the latter symmetry, i.e., Eq. (14), prohibits any matrix elements between $\gamma_{0,5}$ and $\gamma_{j5} (j=1,\ldots,4)$ in the right-hand side of Eq. (12). Namely, the 6×6 matrix $\hat{\Delta}$ in its right-hand side takes the following form:

$$\hat{\Delta} \equiv \begin{bmatrix} \Delta_{00} & \Delta_{05} & \mathbf{0} \\ \Delta_{50} & \Delta_{55} & \mathbf{0} \\ \mathbf{0} & \mathbf{0} & \hat{\Delta}_a \end{bmatrix}, \tag{15}$$

with

$$\hat{\Delta}_a \equiv \begin{bmatrix} \Delta_{1515} & \cdots & \Delta_{1545} \\ \vdots & \ddots & \vdots \\ \Delta_{4515} & \cdots & \Delta_{4545} \end{bmatrix}. \tag{16}$$

This is because $\hat{\gamma}_{0,5}$ are even under $\mathcal{I}$, while $\hat{\gamma}_{j5} (j=1,2,3,4)$ are odd. In order that the Gaussian integral in Eq. (10) converges, all the eigenvalues of $\hat{\Delta}$ have to be positive. Accordingly, the matrix elements described in Eqs. (15) and (16) must obey the following inequalities:

$$\Delta_{00}\Delta_{55} > \Delta_{05}\Delta_{50} = \Delta_{05}^2,$$

$$\Delta_{00} + \Delta_{55} > 0, \quad \mathrm{Tr}\hat{\Delta}_a > 0, \ldots . \tag{17}$$

We can study the effects of these general $\mathcal{T}$-invariant on-site-type random potentials, without any further assumptions. As will be partly shown in Appendix A, however, such an analysis becomes very cumbersome and lengthy. Thus, we henceforth consider only the chemical-potential-type disorder Δ_{00} because it is expected to be dominant among various types of disorder. Those who are interested in the effects of other components such as Δ_{05}, Δ_{55} and $\hat{\Delta}_a$ may consult Appendix A. In Appendix A we have studied the effect of the $\mathcal{T}$-reversal invariant on-site-type disorder on a general ground, focusing on the zero-energy wave function at the critical point.

Being translationally invariant as in Eq. (13), the averaged Green's functions can be readily Fourier transformed by the use of the crystal momentum k. The resulting Green's functions can be expanded in terms of Dirac matrices and its associates,

$$\hat{G}^R(k,\mu) \equiv \sum_{j \in \{0,1,\cdot,5,15,\cdots,42\}} \overline{\mathbf{F}}_j(k,\mu) \hat{\gamma}_j. \tag{18}$$

$\overline{\mathbf{F}}_i(k,\mu)$ stands for some complex-valued function of k and μ. In this momentum representation, $\mathcal{T}$ and $\mathcal{I}$ invariance, i.e., Eqs. (9) and (14), read as follows:

$$\hat{\sigma}_x \otimes \hat{1} \cdot \hat{G}^{R(A)}(k,\mu) \cdot \hat{\sigma}_x \otimes \hat{1} = \hat{G}^{R(A)}(-k,\mu), \tag{19}$$

$$\hat{1} \otimes \hat{s}_y \cdot \hat{G}^{R(A)}(k,\mu) \cdot \hat{1} \otimes \hat{s}_y = \{\hat{G}^{R(A)}\}^t(-k,\mu). \tag{20}$$

These two symmetries require that $\overline{\mathbf{F}}_{i=1,\ldots,4}(k,\mu)$ are odd functions of k, $\overline{\mathbf{F}}_{0,5}$ are even functions of k, and also that $\overline{\mathbf{F}}_{ij} \equiv 0$ for $i \neq j$ and $i,j=1,\ldots,5$. Namely, the retarded and advanced Green's functions are given only in terms of the anticommuting Dirac matrices,

$$\hat{G}^R(k,\mu) \equiv \overline{\mathbf{F}}_0(k,\mu)\hat{1} + \sum_{\mu=1}^{5} \overline{\mathbf{F}}_\mu(k,\mu)\hat{\gamma}_\mu, \tag{21}$$

$$\hat{G}^A(k,\mu) \equiv \overline{\mathbf{F}}_0^*(k,\mu)\hat{1} + \sum_{\mu=1}^{5} \overline{\mathbf{F}}_\mu^*(k,\mu)\hat{\gamma}_\mu. \tag{22}$$

In addition to the $\mathcal{T}$ symmetry and $\mathcal{I}$ symmetry, the *pseudospin rotational symmetry* is also recovered *after the quenched average*. This is because only the chemical-potential-type disorder Δ_{00} is considered now. Specifically, the one-point Green's function after the quenched average respects the simultaneous rotations of the spatial coordinate *and* the pseudospin coordinate,

$$\hat{U}_{n,\phi} \cdot \hat{G}^{R(A)}(k,\mu) \cdot \hat{U}_{n,\phi}^\dagger \equiv \hat{G}^{R(A)}(R_{n,\phi}k,\mu),$$

$$\hat{U}_{n,\phi} \equiv e^{(\phi/4)\epsilon_{\mu\nu\rho} n_\mu \hat{\gamma}_\nu \hat{\gamma}_\rho}. \tag{23}$$

μ, ν, and ρ above run over 1, 2, and 3. $R_{n,\phi}$ in the right-hand side stands for the spatial rotation around the vector n by the angle ϕ. When combined with Eqs. (19) and (20), this rotational symmetry further restricts the form of the Green's functions. For example, the coefficient of $\hat{\gamma}_4$ should be an odd function of k due to Eq. (19), while it should be an even function of k because of Eq. (23). As such, the Green's functions cannot contain $\hat{\gamma}_4$ component under these two symmetry requirements. Moreover, Eq. (23) by itself compels $\overline{\mathbf{F}}_{1,2,3}(k,\mu)$ to be transformed as a vector under the rotation in the k space,

$$\overline{\mathbf{F}}_\mu(k,\mu) \equiv c_1 k_\mu + c_3 k^2 k_\mu + \cdots , \tag{24}$$

with $\mu=1,2,3$.

So far, we have imposed several generic symmetries such as $\mathcal{T}$ symmetry and $\mathcal{I}$ symmetry on the Green's function after the quenched averaged. As a result of this, the Green's function is given only in terms of the Dirac matrices. Since these five Dirac matrices are all anticommuting with one another, the inverse of the Green's function can be easily calculated,

$$\hat{G}^{R,-1}(k,\mu) \equiv \mathbf{F}_0(k,\mu)\hat{1} + \sum_{\nu=1}^{5} \mathbf{F}_\nu(k,\mu)\hat{\gamma}_\nu, \tag{25}$$

$$\overline{\mathbf{F}}_0 = \frac{\mathbf{F}_0}{\mathbf{F}_0^2 - \sum_{\mu=1}^{5} \mathbf{F}_\mu^2}, \quad \overline{\mathbf{F}}_\nu = -\frac{\mathbf{F}_\nu}{\mathbf{F}_0^2 - \sum_{\mu=1}^{5} \mathbf{F}_\mu^2}. \tag{26}$$

Correspondingly, the inverse of the bare Green's function is given as follows:

$$\hat{G}_0^{R,-1}(k,\mu) = (\mu + i\delta)\hat{1} - \sum_{\lambda=1,2,3} k_\lambda \hat{\gamma}_\lambda + m\hat{\gamma}_5 \equiv \sum_{\lambda=0,\cdots,5} \mathbf{f}_\lambda \hat{\gamma}_\lambda. \tag{27}$$

Based on these simplifications, we will derive in Secs. III and IV the electronic property of the disordered single copy of 3+1 Dirac fermion described by Eq. (5). Before finalizing this section, however, it would be appropriate to summarize the engineering dimension of the various quantities introduced in this section. Comparing the impurity Hamiltonian with the pure Hamiltonian, one can first see that

$$m, k_\mu, \mu, \mathbf{f}_\mu, \mathbf{F}_\mu, v_i \sim [L^{-1}], \ \overline{\mathbf{F}}_\mu \sim [L], \tag{28}$$

where L denotes the dimension of a length. Out of this, we can further figure out the engineering dimension of Δ_{jm},

$$\Delta_{jm} \sim [L], \tag{29}$$

by requiring $P[v]$ in Eq. (11) to be dimensionless.

III. SELF-CONSISTENT BORN APPROXIMATION

The scB approximation simply equates the right-hand sides of the following two:

$$\hat{\Sigma}^R(k,\mu) \equiv \hat{G}_0^{R,-1} - \hat{G}^{R,-1}, \equiv (\mathbf{f}_0 - \mathbf{F}_0)\hat{1} + \sum_{\nu=1}^{5} (\mathbf{f}_\nu - \mathbf{F}_\nu)\hat{\gamma}_\nu, \tag{30}$$

$$\hat{\Sigma}^R(k,\mu) = \Delta_{00}\int d^3k' \hat{G}^R(k',\mu) = \Delta_{00}\int_{0<|k|<\Lambda} d^3k' \{\overline{\mathbf{F}}_0(k',\mu)\hat{\gamma}_0 + \overline{\mathbf{F}}_5(k',\mu)\hat{\gamma}_5\}. \tag{31}$$

We have already omitted those terms proportional to $\overline{\mathbf{F}}_{1,2,3,4}(k',\mu)$ in the integrand of Eq. (31) since they are odd functions of k'. Comparing the coefficients of each γ matrix in Eqs. (30) and (31), we can make the closed coupled equation for $\mathbf{F}_0$ and $\mathbf{F}_5$,

$$\Delta_{00}\int_{0<|k|<\Lambda} d^3k \frac{\mathbf{F}_0}{\mathbf{F}_0^2 - \mathbf{F}_5^2 - k^2} = \mathbf{f}_0 - \mathbf{F}_0, \tag{32}$$

$$-\Delta_{00}\int_{0<|k|<\Lambda} d^3k \frac{\mathbf{F}_5}{\mathbf{F}_0^2 - \mathbf{F}_5^2 - k^2} = \mathbf{f}_5 - \mathbf{F}_5 \tag{33}$$

by the use of Eq. (26). We have already used the following relations also:

$$\mathbf{F}_{1,2,3} \equiv \mathbf{f}_{1,2,3} = -k_{1,2,3}, \quad \mathbf{F}_4 \equiv \mathbf{f}_4 \equiv 0. \tag{34}$$

These integral equations in Eqs. (32) and (33) clearly depend on the ultraviolet cutoff Λ. Thus, rescaling the momentum by this cutoff Λ, let us introduce the *dimensionless quantities*, instead of $\mathbf{F}_\mu$, $\mathbf{f}_\mu$, and Δ_{00}. Equations (28) and (29) indicate that they should be rescaled in the following way:

$$\mathbf{F}_{0,5} \to F_{0,5} \equiv \mathbf{F}_{0,5}\Lambda^{-1}, \tag{35}$$

$$\mathbf{f}_{0,5} \to f_{0,5} \equiv \mathbf{f}_{0,5}\Lambda^{-1}, \tag{36}$$

$$\Delta_{00} \to \alpha \equiv 2\pi\Delta_{00}\Lambda. \tag{37}$$

The factor 2π in the definition of α is just for later convenience. In terms of these dimensionless quantities, the above coupled nonlinear equations become

$$(1 + \alpha G)F_0 = f_0 \equiv \mu \pm i\delta, \tag{38}$$

$$(1 - \alpha G)F_5 = f_5 \equiv m, \tag{39}$$

where μ and m in the right-hand side are supposed to be also normalized by Λ^{-1}. G used in the left-hand side was also made dimensionless,

$$G \equiv 2\int_{0<k<1} \frac{1}{(a+ib)^2 - k^2} k^2 dk, \tag{40}$$

$$(a+ib)^2 \equiv F_0^2 - F_5^2. \tag{41}$$

Equations (38)–(41) thus determine F_0 and F_5 as a function of their bare values: f_0 and f_5. F_μ thus obtained should be by definition much smaller than the "ultraviolet cutoff" 1,

$$F_\mu \ll 1. \tag{42}$$

This also leads to $a, b \ll 1$. In the following, we will frequently take full advantage of their smallness, which is always self-consistently verified later (see below).

In Sec. III A, we will present the solution of this coupled equation for general μ and m. Before doing this, however, it would be appropriate to express the imaginary part and real part of G in terms of a and b so that one can roughly estimate these two quantities in small a and b. The real part and the imaginary part of G read as follows:

$$\mathrm{Re}\, G \equiv -2 - \frac{a}{2}\log\left[\frac{(1-a)^2+b^2}{(1+a)^2+b^2}\right] + b\left(\arctan\left[\frac{1-a}{b}\right] + \arctan\left[\frac{1+a}{b}\right]\right), \tag{43}$$

$$\mathrm{Im}\, G \equiv -\frac{b}{2}\log\left[\frac{(1-a)^2+b^2}{(1+a)^2+b^2}\right] - a\left(\arctan\left[\frac{1-a}{b}\right]+\arctan\left[\frac{1+a}{b}\right]\right). \quad (44)$$

Observing these two, please notice that the final two terms in Eqs. (43) and (44), which are proportional to arctan, are nothing but the pole contribution. Namely, the limit $b\to 0$ reduces them to a finite constant with its sign identical to that of b, e.g.,

$$\arctan\left(\frac{1-a}{b}\right)+\arctan\left(\frac{1+a}{b}\right)\to \pi\,\mathrm{sgn}(b),$$

where one should also note that $a,b\ll 1$. Bearing these in mind, one can then evaluate the leading order of Re G and Im G with respect to small a and b,

$$\mathrm{Re}\, G = -2+\pi|b|+\mathcal{O}(a^2), \quad (45)$$

$$\mathrm{Im}\, G = -\,\mathrm{sgn}(b)\pi a+\mathcal{O}(ab). \quad (46)$$

Namely, the second member of Eq. (45) and the first member of Eq. (46) are nothing but the pole contributions mentioned above.

A. Solution for scB equations

1. $m=\mu=0$ case

For the warming up, consider first the case with $\mu=m=0$, i.e., the zero-energy state at the critical point. Equations (38)–(41) have three types of solutions,

$$\text{(i)}\quad F_0=F_5=0, \quad (47)$$

$$\text{(ii)}\quad 1+\alpha G=0\cap F_5=0, \quad (48)$$

$$\text{(iii)}\quad 1-\alpha G=0\cap F_0=0. \quad (49)$$

Observing the estimates given in Eqs. (45) and (46), please notice that type-(iii) solution cannot be satisfied for $\alpha>0$ and $a,b\ll 1$. Thus, we will ignore this henceforth.

The type-(i) solution is always trivially satisfied. This solution indicates that the zero-energy state is not renormalized at all by the disorder, $F_0=f_0=0$, $F_5=f_5=0$. Thus, it describes the *diffusionless* zero-energy state.

The type-(ii) solution is a nontrivial solution, which turns out to describe the *diffusive* zero-energy state. To see this, let us begin with the first condition of Eq. (48), i.e., $1+\alpha G=0$. The imaginary part of this gives Im $G=0$, which is satisfied either when $a=0$ or when $b=0$ and $|a|>1$ (see Fig. 4). Since $a,b\ll 1$ as noted earlier, the only physical solution satisfying Im $G=0$ is thus $a=0$. The remaining condition, $1+\alpha$ Re $G=0$, becomes then simple,

$$b\,\arctan[b^{-1}]=1-\frac{1}{2\alpha}. \quad (50)$$

Since $F_5=0$ gives $a+ib=F_0$, a and b thus obtained stand for the renormalized chemical potential $\bar{\mu}$ and the inverse of the lifetime τ^{-1}, respectively. Accordingly, the type-(ii) solution simply denotes that the zero-energy state acquires a finite lifetime τ, while its chemical potential is free from renormalizations,

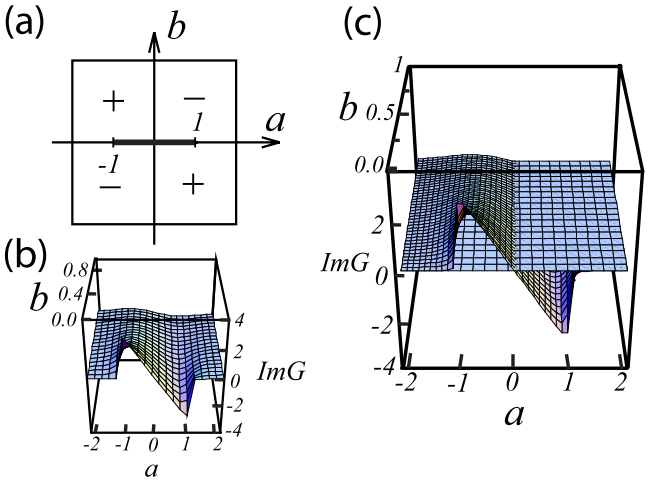

FIG. 4. (Color online) Im G as a function of a and b. (a) The sign of Im G is denoted by "+(−)" at the four regions, i.e., $a,b>0$, $a>0>b$, $b>0>a$, and $0>a,b$. Im G is an odd function both in a and in b. The bold line which runs from (−1,0) to (1,0) denotes a sort of the branch cut. Namely, Im G jumps from $-2\pi^2 a$ to $+2\pi^2 a$ (from $b=+0$ to $b=-0$). (b) A side view plot of Im G only for $b>0$. (c) Im $G\equiv 0$ is satisfied either when $a=0$, or when $b=0$ and $|a|>1$.

$$\bar{\mu}=0,\quad \tau^{-1}\arctan[\tau]=1-\frac{\alpha_c}{\alpha}. \quad (51)$$

Namely, for $\alpha>\alpha_c\equiv\frac{1}{2}$, τ^{-1} can take a finite value.

For a weak disorder region ($\alpha<\alpha_c$), Eq. (51) cannot be satisfied for any τ. Thus, the only solution therein is the type-(i) trivial solution. On the other hand, both the type-(i) solution and type-(ii) solution become possible above this critical disorder strength ($\alpha>\alpha_c$). In the next three paragraphs, we will determine which solution is *physically sensible* for $\alpha>\alpha_c$.

To do this, we will extend these two solutions into a small but finite μ region. Namely, by seeing how this chemical potential will be renormalized for each case, we will judge which solution is the physical one for $\alpha>\alpha_c$. Recall first that $F_5=0$ in either case. Thus, a and b correspond to $\bar{\mu}$ and τ^{-1}, respectively, so that a and b should be an odd and an even function of the bare chemical potential μ, respectively.

Bearing these in mind, let us extend the type-(i) solution into a small μ region first. Namely, keeping the leading order in small μ, we can evaluate the real part of Eq. (38),

$$(1-2\alpha)a+\mathcal{O}(\mu^3)=\mu, \quad (52)$$

where we used $a\propto\mathcal{O}(\mu)$ and $b\propto\mathcal{O}(\mu^2)$. Thus, the renormalized chemical potential is estimated up to $\mathcal{O}(\mu)$ as follows:

$$\bar{\mu} \equiv a = \frac{\mu}{1-2\alpha} + \mathcal{O}(\mu^3), \tag{53}$$

while b will be determined up to $\mathcal{O}(\mu^2)$ from the imaginary part of Eq. (38),

$$\tau^{-1} \equiv b = \frac{\alpha\pi}{(1-2\alpha)^3}\mu^2 + \mathcal{O}(\mu^4). \tag{54}$$

This solution indicates that the negative eigenenergy state and the positive eigenenergy state are *inverted* energetically for $\alpha > \alpha_c$: sign $\bar{\mu}$=−sign μ. This is, however, clearly unphysical at least for small μ.

When the type-(ii) solution is extended into a small μ region, a similar algebra gives us the following expression for the real part of Eq. (38) up to $\mathcal{O}(\mu)$:

$$(1-2\alpha)a + 4\alpha\tau^{-1}\arctan[\tau]a = \mu. \tag{55}$$

In this equation, we have already made implicit those contributions proportional to $\mathcal{O}(\mu^3)$ and $\mathcal{O}(\tau^{-2}\mu)$ while keeping those proportional to $\mathcal{O}(\tau^{-1}\mu)$ explicit. Please also note that we have used $a \propto \mathcal{O}(\mu)$ and $b = \tau^{-1} + \mathcal{O}(\mu^2)$. Namely, contrary to the type-(i) solution, b converges to a *nonzero* τ^{-1} at the leading order in small μ. As a result of this, Eq. (55) has acquired an additional $\mathcal{O}(\mu)$ term, i.e., $4\alpha\tau^{-1}\arctan[\tau]\cdot a$, which was absent in Eq. (52). This additional term makes the sign of $\bar{\mu}$ to be same as that of μ. Namely, by the use of $1-2\alpha = -2\alpha\tau^{-1}\arctan[\tau] + \mathcal{O}(\mu^2)$, Eq. (55) leads us to

$$(2\alpha - 1)a + \mathcal{O}(\mu^3) = \mu. \tag{56}$$

Out of this, one can evaluate the renormalized chemical potential up to $\mathcal{O}(\mu)$ as follows:

$$\bar{\mu} \equiv a = \frac{\mu}{2\alpha - 1} + \mathcal{O}(\mu^3), \tag{57}$$

whose sign is clearly same as that of the bare one for $\alpha > \alpha_c$: sgn $\bar{\mu}$=sgn μ. Observing these two distinct behaviors for the finite μ region, i.e., Eqs. (53) and (57), we conclude that for $\alpha > \alpha_c$, the type-(ii) solution is the physically sensible solution.

To summarize so far, the physical solutions obtained at $m=\mu=0$ are twofold, depending on the disorder strength α. When $\alpha < \alpha_c = 1/2$, the type-(i) trivial solution is the only possible solution,

$$\text{(i)}\quad F_0 = F_5 = 0 \quad \text{for} \quad \alpha < \alpha_c. \tag{58}$$

This means that the electronic state at the zero energy is free from the disorder up to a certain critical disorder strength.

On the other hand, when its strength exceeds this critical value, i.e., $\alpha > \alpha_c$, the type-(ii) solution should be adopted,

$$\text{(ii)}\quad F_0 = i\tau^{-1},\ F_5 = 0 \quad \text{for} \quad \alpha > \alpha_c. \tag{59}$$

This solution means that the electronic state at the zero energy acquires a finite lifetime τ defined by Eq. (51).

2. μ=0 *and finite m case*

Let us introduce a finite topological mass m into Eq. (58) and (59), respectively, with the chemical potential μ being still zero. We will first argue that the solution of Eqs. (38)–(41) in the presence of the finite mass is uniquely determined for $\alpha < \alpha_c$. Such a solution reads

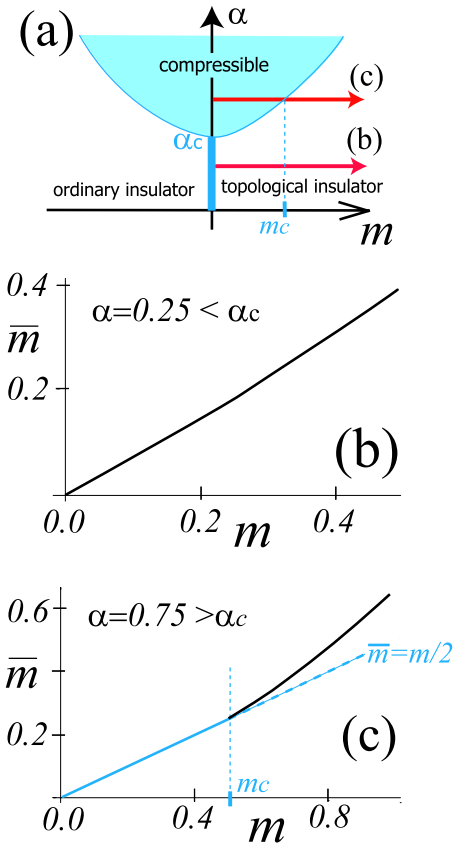

FIG. 5. (Color online) (a) A schematic phase diagram at μ=0. The white region corresponds to the incompressible phase, where no finite DOS exists at μ=0. In the compressible phase (blue shaded region) a finite DOS exists at μ=0, i.e., Eq. (64). (b) The renormalized mass $\bar{m}$ as a function of the bare mass m for $\alpha = 0.25 < \alpha_c$. (c) $\bar{m}$ as a function of m for $\alpha = 0.75 > \alpha_c$. There exists the critical value of the bare mass m, below which $\bar{m} = m/2$, and above which $\bar{m}$ is determined by Eq. (61).

$$F_0 = 0, \quad F_5 = \bar{m}, \tag{60}$$

where $\bar{m}$ is given as a function of the bare mass,

$$\bar{m}\{1 + 2\alpha - 2\alpha\bar{m}\arctan[\bar{m}^{-1}]\} = m. \tag{61}$$

A typical behavior of $\bar{m}$ as a function of the bare mass is depicted in Fig. 5(b).

To see that Eqs. (60) and (61) is the only possible solution for $\alpha < \alpha_c$, let us begin with the real part of $1+\alpha G$ appearing in Eq. (38). In the case of $\alpha < \alpha_c$, it is always positive definite for any $a < 1$. As such, we must take F_0 to be zero, to satisfy Eq. (38). This leads to $F_5 = b - ia$. Using this, consider next the imaginary part of Eq. (39),

$$(1 - \alpha\,\mathrm{Re}\,G)\cdot a + \alpha\,\mathrm{Im}\,G\cdot b = 0. \tag{62}$$

Observing the leading-order estimates of Re G and Im G, i.e., Eqs. (45) and (46), one can further see that Eq. (62)

uniquely leads to $a=0$. The remaining condition, i.e., the real part of Eq. (39), then becomes simple,

$$(1-\alpha\,\mathrm{Re}\,G)\cdot b=(1+2\alpha-2\alpha b\,\arctan[b^{-1}])\cdot b=m.$$

Now that $(F_0,F_5)\equiv(0,b)$, this equation is nothing but Eq. (61) when b replaced by $\bar{m}$.

Let us next consider the case of $\alpha>\alpha_c$. The solution of Eqs. (38)–(41) in this case is twofold; we have a certain critical mass value m_c, which is given as a function of α,

$$m_c\equiv 2\tau^{-1},\quad \tau^{-1}\arctan[\tau]\equiv 1-\frac{\alpha_c}{\alpha}. \tag{63}$$

When the topological mass is less than this critical value ($m<m_c$), the solution of Eqs. (38)–(41) becomes

$$F_0=+i\sqrt{\tau^{-2}-\bar{m}^2},\quad F_5=\bar{m}\equiv\frac{m}{2}, \tag{64}$$

where τ was already defined in Eq. (63). On the other hand, when the topological mass exceeds this critical value ($m>m_c$), the solution becomes Eqs. (60) and (61) again.

To see that Eq. (64) is the solution of Eqs. (38)–(41) for $\alpha>\alpha_c$ and $m<m_c$, take $1+\alpha G\equiv 0$ first so that Eq. (38) is satisfied. By the use of the same arguments described above Eq. (50), this immediately gives us $(a,b)\equiv(0,\tau^{-1})$, with τ being defined by Eq. (51). Since $1-\alpha G\equiv 2$, Eq. (39) leads to $F_5\equiv m/2$. Thus, using these two things, we obtain F_0 out of Eq. (41), which is nothing but Eq. (64). When m exceeds $m_c\equiv 2\tau^{-1}$, Eq. (64) becomes an unphysical solution in a similar way as the type-(i) solution in Sec. III A 1 did for $\alpha>\alpha_c$,

$$F_0=\pm\sqrt{\bar{m}^2-\tau^{-2}},\ F_5=\bar{m}\equiv\frac{m}{2}.$$

Instead of this, it turns out that we should adopt the other solution for $m>m_c$, i.e., Eqs. (60) and (61).

A typical behavior of $\bar{m}$ in the case of $\alpha>\alpha_c$ is depicted in Fig. 5(c), where these two solutions, i.e., Eq. (64) and Eqs. (60) and (61), are indeed connected continuously at $m=m_c$. Since Eq. (64) always supports a finite density of state (DOS), we can regard that the compressible phase extends over $\alpha>\alpha_c$ and $m<m_c$. On the other hand, Eqs. (60) and (61) do not support any finite DOS. As such, we can regard that an incompressible phase extends over $\alpha<\alpha_c$ or $m>m_c$ [Fig. 5(a)].

3. General μ and m case

For finite μ and m, both F_0 and F_5 are in general nonzero and we cannot solve Eqs. (38)–(41) analytically. Accordingly, we have numerically solved the coupled equations with respect to a and b so that F_0 and F_5 are derived in terms of μ and m.

Before describing the numerical solution, let us first argue about the generic features of such solutions. Notice first that Re G is an even function of both a and b, while Im G is an odd function of both a and b. Thus the following two should be degenerate at any given μ and m as the solutions of Eqs. (38)–(41):

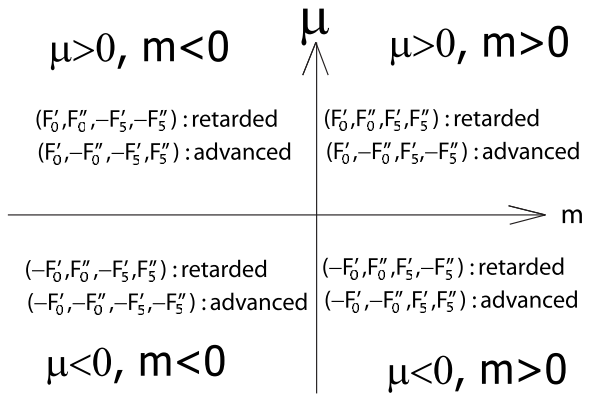

FIG. 6. F_0 and F_5 as a function of m and μ. F_j' and F_j'' are the real and imaginary parts of a function F_j. At any parameter point, we generally have at least two solutions, which correspond to the retarded Green's function and advanced one.

$$(F_0',F_0'',F_5',F_5''),\quad (F_0',-F_0'',F_5',-F_5''), \tag{65}$$

where F_j' and F_j'' are the real and imaginary parts of F_j. Namely, these two solutions correspond to the retarded Green's function and advanced one, respectively.

The above two solutions at given m and μ can be further extended into the other three quadrants, i.e., $(-m,\mu)$, $(m,-\mu)$, and $(-m,-\mu)$,

$$\begin{aligned}(F_0',\pm F_0'',F_5',\pm F_5'')_{|m,\mu}&=(F_0',\pm F_0'',-F_5',\mp F_5'')_{|-m,\mu}\\&=(-F_0',\pm F_0'',F_5',\mp F_5'')_{|m,-\mu}\\&=(-F_0',\pm F_0'',-F_5',\pm F_5'')_{|-m,-\mu},\end{aligned}$$

where the upper sign corresponds to the retarded function for any of these four regions by construction (Fig. 6). Observing this, please notice that both F_5' and F_5'' vanish at $m=0$, which is indeed the case with Sec. III A 1. Similarly, one can also see that F_0' and F_5'' should vanish at $\mu=0$ for any m. Both Eqs. (60) and (61) and Eq. (64) actually observe this.

These considerations are also consistent with the numerical solution. In Figs. 7 and 8, we demonstrated numerically how F_0 and F_5 behave as a function of μ and m (only for the first quadrant, $m>0$ and $\mu>0$), at specific values of α. Figure 7 is for $\alpha<\alpha_c$, while Fig. 8 is for $\alpha>\alpha_c$. In the limit of $\mu\to 0$, F_0 and F_5 in these two figures continuously connect with the two analytic solutions previously derived, i.e., Eqs. (60) and (61) and Eq. (64), respectively.

We have also checked that whenever $F_0''=F_5''\equiv 0$, F_5' is always greater than F_0', i.e., $a^2-b^2<0$. As such, the spectral function is identically zero, provided that both F_0'' and F_5'' vanish. Such a phase should be regarded as an incompressible phase having no bound states. On the one hand, when either F_0'' or F_5'' is finite, the spectral weight is finite and such a phase is compressible.

By seeing whether F_0'' and F_5'' totally vanishes or not, we have determined the phase diagram in the μ-m-α space. The phase boundaries between the compressible phase and the incompressible phase thus obtained are schematically drawn

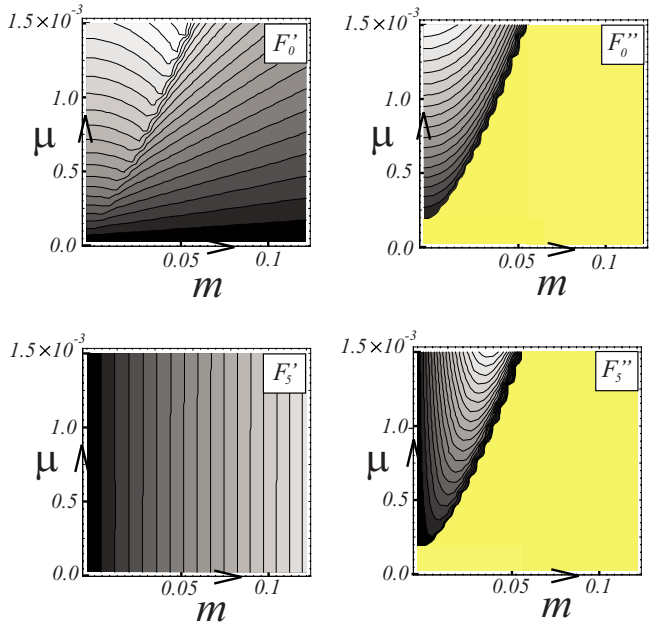

FIG. 7. (Color online) $\alpha=0.48$; (a) The contour plot of F_0' as a function of $\mu>0$ and $m>0$. The value of F_0' decreases toward the dark region, and becomes zero at $\mu=0$. The contour interval is 1.2×10^{-3}. (b) The contour plot of F_0''. The value of F_0'' decreases toward the darker region, and becomes zero at the incompressible phase (yellow region). The contour interval is 0.6×10^{-3}. (c) The contour plot of F_5'. F_5' decreases toward the darker region, and becomes zero at $m=0$. The contour interval is 4.0×10^{-3}. (d) The contour plot of F_5''. F_5'' increases toward the darker region and becomes zero at $\mu=0$, $m=0$ and the incompressible phase (yellow region). The contour interval is -1.2×10^{-5}.

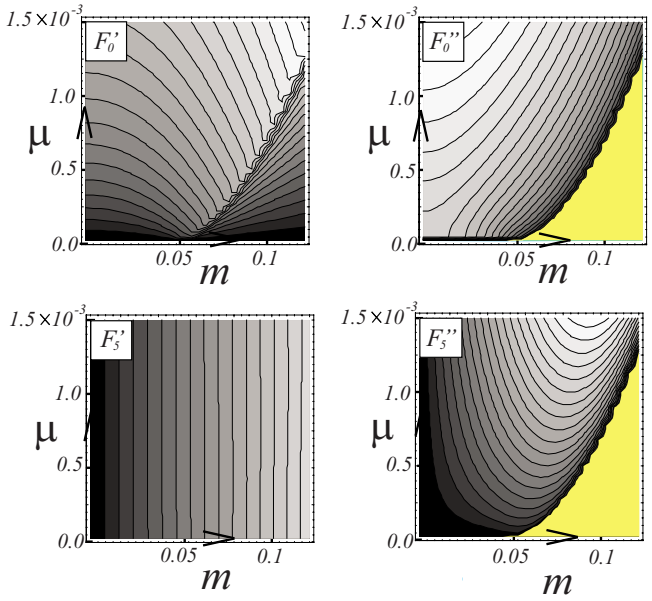

FIG. 8. (Color online) $\alpha=0.52$; (a) The contour plot of F_0' as a function of $\mu>0$ and $m>0$. The value of F_0' decreases toward the dark region, and becomes zero at $\mu=0$. The contour interval is 1.8×10^{-3}. (b) The contour plot of F_0''. The value of F_0'' decreases toward the darker region, and becomes zero at the incompressible phase (yellow region). The contour interval is 1.8×10^{-3}. (c) The contour plot of F_5'. F_5' decreases toward the darker region, and becomes zero at $m=0$. The contour interval is 4.0×10^{-3}. (d) The contour plot of F_5''. F_5'' increases toward the darker region and becomes zero at $\mu=0$, $m=0$ and the incompressible phase (yellow region). The contour interval is -3.0×10^{-5}.

in Fig. 9, while accurately specified in Fig. 10. For $\alpha>\alpha_c$, we have a finite critical mass value, i.e., m_c, below which a compressible phase extends even at $\mu=0$ [Fig. 9(c) and Figs. 10(e) and 10(f)]. This critical value goes to zero when α goes to α_c from above [Fig. 10(d)]. For $\alpha<\alpha_c$, we have a compressible region not in the $\mu=0$ region anymore, but still in the nonzero μ region [Fig. 9(b) and Figs. 10(a)–10(c)]. The slope of the phase boundary in $\alpha<\alpha_c$, given as follows:

$$\left.\frac{d\mu_c}{dm_c}\right|_{\mu_c=m_c=0} \equiv \frac{1-2\alpha}{1+2\alpha},$$

increases when the disorder strength decreases [Figs. 10(a)–10(c)].

IV. DIFFUSON AND QUANTUM CONDUCTIVITY CORRECTION

In Sec. III, we have derived the one-point Green's function within the self-consistent Born approximation. In the 3D parameter space spanned by μ, m, and α, we have observed that the topological insulator and an ordinary insulator are always intervened by the compressible phase. The topological insulator supports a single 2+1 surface massless Dirac fermion on each boundary, while an ordinary insulator does not. As such, we expect that this intervening phase is composed by those wave functions which *extend* over an entire bulk (see Sec. I for its reason).

As the first step to understand the nature of this compressible phase especially for $\alpha<\alpha_c$, we will calculate the series sum of the ladder-type diagram $\hat{\Gamma}^d(q,\omega)$ [see Fig. 11(a)], only to see that the diffuson thus obtained consists of two quasidegenerate low-energy modes,

$$\hat{\Gamma}^d(q,\omega) \propto \frac{1}{\omega+iDq^2}\hat{\Gamma}_1^d + \frac{1}{\omega+iDq^2+i\tau_{\text{topo}}^{-1}}\hat{\Gamma}_2^d + \cdots \quad (66)$$

with $\tau_{\text{topo}}^{-1}\propto m^2$. The information of the charge diffusion is solely encoded into the first term, which thus always has the diffusion pole structure. On the other hand, the second term becomes massless only at $m=0$ (but generic μ), while it suffers from the finite infrared cutoff τ_{topo}^{-1} for the finite m case. We will explicitly see that the second term is actually associated with the parity degree of freedom, which, at $m=0$, becomes a conserved quantity of our effective continuum model, i.e., Eq. (5).

When the hole line of $\hat{\Gamma}^d(q,\omega)$ is time reversed, these two-mode features are translated into the backward-scattering channel associated with the "fan"-type diagrams $\hat{U}^{\text{coop}}(k+k',\omega)$ [see Fig. 11(b)]. Namely, for small ω and $k+k'$, it is also dominated by two quasidegenerate dominant contributions,

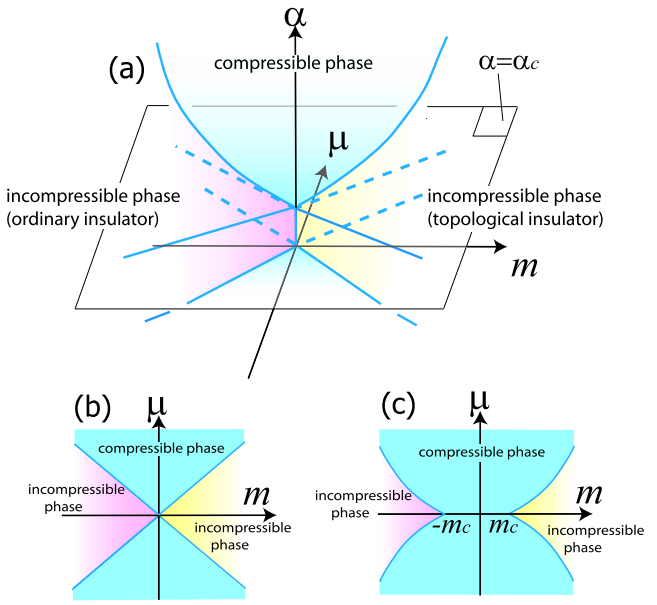

FIG. 9. (Color online) (a) A schematic phase diagram in the μ-m-α space. Either F_0'' or F_5'' always remains finite in the compressible phase (blue), while both of them become zero at the remaining parameter region (incompressible phase), which is further divided into an ordinary insulator (red) and the topological insulator (yellow). (b) A schematic phase diagram in μ-m plane for $\alpha < \alpha_c$, and (c) that for $\alpha > \alpha_c$. These correspond to the numerical results shown in Fig. 10.

$$\hat{U}^{\mathrm{coop}}(k+k',\omega) \propto \frac{1}{\omega + iD(k+k')^2}\hat{U}_1^{\mathrm{c}} + \frac{1}{\omega + iD(k+k')^2 + i\tau_{\mathrm{topo}}^{-1}}\hat{U}_2^{\mathrm{c}} + \cdots . \tag{67}$$

One is obtained from the charge mode channel, i.e., Γ_1^d, with its hole line time reversed, while the other is from the parity mode channel, $\hat{\Gamma}_2^d$. In this section, we will further see that both of these two give rise to the same amplitude of the anti-weak-localization (AWL) correction to the electric conductivity at $m=0$. In the presence of the finite topological mass m, however, the second term in Eq. (67) becomes less dominant because of the finite infrared cutoff $\tau_{\mathrm{topo}}^{-1}$. Namely, half of the AWL correction becomes ineffective on increasing m ("quantum correction doubling").

Using the knowledge obtained in this section, we will propose in Sec. IV the possible microscopic mechanism of how the bulk-critical region emerges between the topological insulator and an ordinary insulator.

This section is organized as follows. In Sec. IV A, we will sum up the entire ladder-type diagram in the particle-hole channel, using the one-point Green's function obtained in the self-consistent Born calculation,

$$\hat{G}^{R,-1}(k;\mu,m) = F_0\hat{1} - k_\nu\hat{\gamma}_\nu + F_5\hat{\gamma}_5, \tag{68}$$

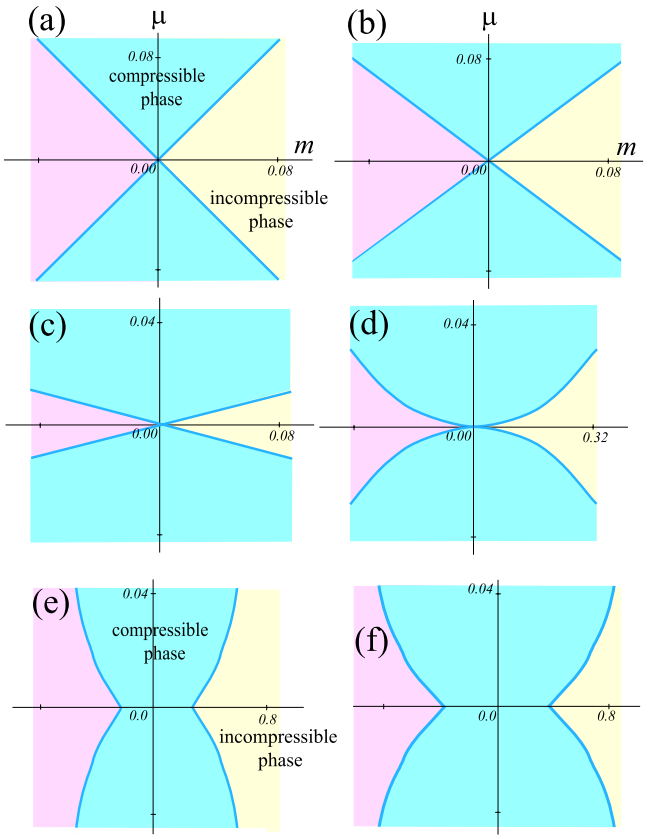

FIG. 10. (Color online) Phase boundaries between the compressible phase and the incompressible (gapped) phase, in the μ-m plane, at several values of α. (a) α=0.0, (b) α=0.1, (c) α=0.4, (d) $\alpha=\alpha_c$=0.5, (e) α=0.6, and (f) α=0.7.

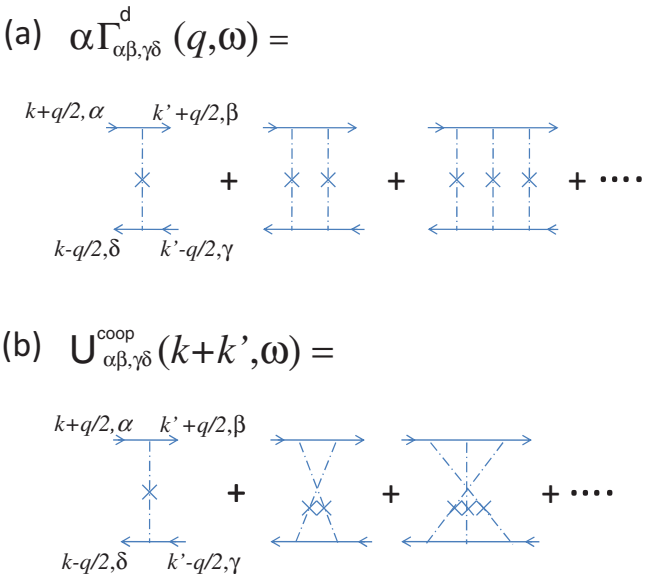

FIG. 11. (Color online) (a) A series sum of the ladder-type diagrams $\Gamma^d_{\alpha\beta,\gamma\delta}(q,\omega)$, (b) A series sum of the "fan"-type diagrams $\hat{U}^{\mathrm{coop}}_{\alpha\beta,\gamma\delta}(k+k',\omega) \equiv \alpha\Sigma_{\delta_1,\gamma_1}\{\hat{1}\otimes\hat{s}_y\}_{\gamma\gamma_1}\hat{\Gamma}^d_{\alpha\beta,\delta_1\gamma_1}(k+k',\omega)\{\hat{1}\otimes\hat{s}_y\}_{\delta_1\delta}$.

$$\hat{G}^{A,-1}(k;\mu,m) = F_0^*\hat{1} - k_\nu\hat{\gamma}_\nu + F_5^*\hat{\gamma}_5, \tag{69}$$

with $F_0 \equiv \bar{\mu} + i\tau^{-1}$ and $F_5 \propto m$. Such a summand should contain those contributions which diverge at $\omega=0$ and $q=0$. We will identify this diverging contribution in Sec. IV B, only to see that $\hat{\Gamma}^d(q,\omega)$ contain two *quasi*degenerate dominant contributions, as in Eq. (66). Explicit expressions for $\hat{\Gamma}_1^d$, $\hat{\Gamma}_2^d$, and τ_{topo}^{-1} will be therefore given here. By calculating the parity-density correlation function, we will show in Sec. IV C that $\hat{\Gamma}_2^d$ solely participates in the parity diffusion mode. Finally, the quantum conductivity corrections arising from these two terms are calculated in Sec. IV D, based on the Kubo formula.

Comparing Eqs. (53) and (54) with Eqs. (57) and (59), notice also that the weak-localization (WL) calculation in this section becomes a controlled analysis only for the weak disorder region, $\alpha < \alpha_c$. Namely, the renormalized chemical potential $\bar{\mu}$ and the lifetime τ^{-1} determined in Sec. III guarantee a sufficiently small $1/\bar{\mu}\tau$ around $\mu \simeq 0$ *only for this weak disorder region*,

$$\bar{\mu}\tau = \frac{1}{\alpha\pi}\frac{(\alpha_c-\alpha)^2}{\alpha_c^2}\frac{1}{\mu} + \mathcal{O}(\mu) \quad \text{for} \quad \alpha < \alpha_c. \tag{70}$$

For the strong disorder region, however, $1/\bar{\mu}\tau$ readily diverges around the zero-energy region,

$$\bar{\mu}\tau = \frac{\pi\alpha_c}{2\alpha}\mu + \mathcal{O}(\mu^3) \quad \text{for} \quad \alpha > \alpha_c. \tag{71}$$

Thus, the noncrossing approximation employed in Sec. III and the corresponding WL calculation described below acquire the small coupling constant $\frac{1}{\bar{\mu}\tau}$, only for $\alpha < \alpha_c$, but, for $\alpha > \alpha_c$, they generally do not. Bearing in mind especially this strong disorder region, we will demonstrate in Appendix B the mode-mode coupling calculation, which is complementary to the weak-localization studies described in this section. Without resorting to the Kubo formula, this theoretical framework gives us the gap equation for the diffusion constant, taking into account the interference effects due to the Cooperon term. The basic feature, which we will observe in this section, such as the quantum correction doubling, are also confirmed by this analysis (see Appendix B).

A. Ladder-type diagrams in the particle-hole channel

For clarity of the following description, let us first define a tensor composed by two 4×4 matrices,

$$\hat{A} \equiv \hat{A}_r \times \hat{A}_a.$$

The former 4×4 matrix $\hat{A}_r$ is for the particle (retarded) line, while the other, i.e., $\hat{A}_a$, is for the hole (advance) line. Throughout this section, we distinguish this "$\times$" mark from the "$\otimes$" mark, latter of which separates the spin space and sublattice space. The product of two tensors is defined as follows:

$$\hat{A}\cdot\hat{B} \equiv \hat{A}_r\hat{B}_r \times \hat{B}_a\hat{A}_a. \tag{72}$$

Note here that the order of the product in the hole line is reversed, compared with that of the left-hand side. Under this algebra, the series sum of the ladder diagram in the particle-hole channel, i.e., Figure 11(a), is just the inverse of the following tensor:

$$\{\hat{1} - \alpha\hat{\Pi}(q,\omega)\}_{\alpha\delta,\gamma\beta} \equiv \left\{\hat{1}\times\hat{1} - \alpha\sum_k \hat{G}^R(0_+)\times\hat{G}^A(0_-)\right\}_{\alpha\delta,\gamma\beta}$$
$$\equiv \delta_{\alpha\delta}\delta_{\gamma\beta} - \alpha\sum_k \hat{G}^R_{\alpha\delta}(0_+)\hat{G}^A_{\gamma\beta}(0_-), \tag{73}$$

with $(0_\pm) \equiv (k \pm \frac{q}{2}, \mu \pm \frac{\omega}{2})$. Namely, the following identity can be readily checked:

$$\{\hat{1} - \alpha\hat{\Pi}(q,\omega)\}_{\alpha\alpha_1,\beta_1\beta}\Gamma^d_{\alpha_1\delta,\gamma\beta_1}(q,\omega) \equiv \delta_{\alpha\delta}\delta_{\gamma\beta}. \tag{74}$$

Notice also that we have already normalized the momentum by the ultraviolet cutoff Λ as in Eqs. (35)–(37) so that $\alpha \equiv 2\pi\Delta_{00}\Lambda$ and $\Sigma_k \equiv 2\int_0^1 k^2 dk$. This notation also holds true for Eqs. (78), (92), and (93).

For simplicity of the explanation, we will calculate the inverse of Eq. (73), with q taken to be zero from the beginning [see also the description around Eq. (99)]. Such an inverse diverges if $\omega=0$, while it does not for general ω. When q taken to be zero, the polarization part becomes simple,

$$\{\hat{1} - \alpha\hat{\Pi}(q\equiv 0,\omega)\}_{\alpha\delta,\gamma\beta} \equiv a_0\hat{1} + a_1\hat{T}_1 + a_2\hat{T}_2 + a_3\hat{T}_3 + a_4\hat{T}_4, \tag{75}$$

$$T_1 \equiv \sum_{\mu=1}^{3}\hat{\gamma}_\mu\times\hat{\gamma}_\mu, \quad \hat{T}_2 \equiv \hat{1}\times\hat{\gamma}_5, \tag{76}$$

$$\hat{T}_3 \equiv \hat{\gamma}_5\times\hat{1}, \quad \hat{T}_4 \equiv \hat{\gamma}_5\times\hat{\gamma}_5. \tag{77}$$

Namely, it is just a linear combination of the five tensors with their coefficients defined as follows:

$$(a_0,a_1,a_2,a_3,a_4) \equiv \left\{1 - \alpha\sum_k \frac{F_{0+}F_{0-}^*}{(k^2 - F_{0+}^2 + F_{5+}^2)[k^2 - (F_{0-}^*)^2 + (F_{5-}^*)^2]}, \; -\alpha\sum_k \frac{k_x^2}{(k^2 - F_{0+}^2 + F_{5+}^2)[k^2 - (F_{0-}^*)^2 + (F_{5-}^*)^2]}, \right.$$
$$\alpha\sum_k \frac{F_{0+}F_{5-}^*}{(k^2 - F_{0+}^2 + F_{5+}^2)[k^2 - (F_{0-}^*)^2 + (F_{5-}^*)^2]}, \; \alpha\sum_k \frac{F_{5+}F_{0-}^*}{(k^2 - F_{0+}^2 + F_{5+}^2)[k^2 - (F_{0-}^*)^2 + (F_{5-}^*)^2]},$$
$$\left. -\alpha\sum_k \frac{F_{5+}F_{5-}^*}{(k^2 - F_{0+}^2 + F_{5+}^2)[k^2 - (F_{0-}^*)^2 + (F_{5-}^*)^2]}\right\}. \tag{78}$$

The $\pm$ subscripts on F_i above mean that the argument of $F_i(\mu)$ is shifted by $\pm\frac{\omega}{2}$,

$$F_{i\pm} \equiv F_i\left(\mu \pm \frac{\omega}{2}\right).$$

As such, a_0, a_1, and a_4 become real valued at $\omega=0$, while a_2 and a_3 become complex conjugate with each other,

$$a^*_{0,1,4|\omega=0} = a_{0,1,4|\omega=0}, \quad a^*_{2|\omega=0} = a_{3|\omega=0}. \tag{79}$$

One can evaluate the signs of the former three real-valued quantities by noting that F_μ is much smaller than the ultraviolet cutoff. They read

$$a_{0|\omega=0} > 0, \quad a_{1|\omega=0} < 0, \quad a_{4|\omega=0} \leq 0. \tag{80}$$

Notice also that all the integrands for a_2, a_3, and a_4 contain F_5, which is proportional to the topological mass (see Sec. III). Thus these three quantities vanish when the topological mass m is zero,

$$a_4 \propto \mathcal{O}(m^2), \quad a_{2,3} \propto \mathcal{O}(m). \tag{81}$$

The inverse of Eq. (75) also becomes a linear combination of a finite number of tensors composed of γ matrices because of the cyclic nature; $\gamma_1\gamma_2\gamma_3\gamma_4\gamma_5 \equiv -\gamma_0$,

$$\begin{aligned}\hat{\Gamma}^d(q=0,\omega) \equiv{}& \beta_0\hat{1} + \beta_1\hat{T}_1 + \beta_2\hat{T}_2 + \beta_3\hat{T}_3 + \beta_4\hat{T}_4 + \beta_5\hat{S}_1 \\ &+ \beta_6\hat{S}_2 + \beta_7\hat{T}_4\cdot\hat{T}_1 + \beta_8\hat{T}_2\cdot\hat{S}_1 + \beta_9\hat{T}_3\cdot\hat{S}_1 + \beta_{10}\hat{T}_4\cdot\hat{S}_1 \\ &+ \beta_{11}\hat{T}_4\cdot\hat{S}_2,\end{aligned} \tag{82}$$

where two additional tensors are introduced in the following way:

$$\hat{S}_1 \equiv \hat{\gamma}_1\hat{\gamma}_2 \times \hat{\gamma}_2\hat{\gamma}_1 + \hat{\gamma}_2\hat{\gamma}_3 \times \hat{\gamma}_3\hat{\gamma}_2 + \hat{\gamma}_3\hat{\gamma}_1 \times \hat{\gamma}_3\hat{\gamma}_1,$$

$$\hat{S}_2 \equiv \hat{\gamma}_1\hat{\gamma}_2\hat{\gamma}_3 \times \hat{\gamma}_3\hat{\gamma}_2\hat{\gamma}_1. \tag{83}$$

After lengthy algebra, one can express its 12 coefficients β_j in terms of those of Eq. (75) as follows:

$$\begin{bmatrix}\beta_0\\ \beta_1\\ \beta_2\\ \beta_3\\ \beta_4\\ \beta_5\\ \beta_6\\ \beta_7\\ \beta_8\\ \beta_9\\ \beta_{10}\end{bmatrix} \equiv \frac{1}{8}\begin{bmatrix} -3\delta a_{04} & -\delta a_{04} & -3a_{04} & -a_{04} \\ a_1 & 3a_1 & a_1 & 3a_1 \\ 3\delta a_{23} & \delta a_{23} & 3a_{23} & a_{23} \\ -3\delta a_{23} & -\delta a_{23} & 3a_{23} & a_{23} \\ 3\delta a_{04} & \delta a_{04} & -3a_{04} & -a_{04} \\ \delta a_{04} & -\delta a_{04} & a_{04} & -a_{04} \\ -3a_1 & 3a_1 & -3a_1 & 3a_1 \\ -a_1 & -3a_1 & a_1 & 3a_1 \\ -\delta a_{23} & \delta a_{23} & -a_{23} & a_{23} \\ \delta a_{23} & -\delta a_{23} & -a_{23} & a_{23} \\ -\delta a_{04} & \delta a_{04} & a_{04} & -a_{04} \end{bmatrix}\begin{bmatrix} f_1\\ f_3\\ f_2\\ f_4\end{bmatrix}, \tag{84}$$

$$\beta_{11} \equiv -3a_1^3(f_4^{-1} + f_1^{-1})f_1f_2(-f_3 + f_4), \tag{85}$$

where a_{04}, δa_{04}, a_{23}, δa_{23}, and $f_{1,2,3,4}$ are defined in terms of a_0, a_1, …, and a_4,

$$\delta a_{23} \equiv a_2 - a_3, \quad \delta a_{04} \equiv a_0 - a_4, \tag{86}$$

$$a_{23} \equiv a_2 + a_3, \quad a_{04} \equiv a_0 + a_4, \tag{87}$$

$$f_1 \equiv \frac{1}{a_1^2 + (\delta a_{04} + \delta a_{23})(-\delta a_{04} + \delta a_{23})}, \tag{88}$$

$$f_2 \equiv \frac{1}{a_1^2 + (-a_{04} + a_{23})(a_{04} + a_{23})}, \tag{89}$$

$$f_3 \equiv \frac{1}{9a_1^2 + (\delta a_{04} + \delta a_{23})(-\delta a_{04} + \delta a_{23})}, \tag{90}$$

$$f_4 \equiv \frac{1}{9a_1^2 + (-a_{04} + a_{23})(a_{04} + a_{23})}. \tag{91}$$

B. Identification of the diffusion pole

Using Eqs. (68) and (69), we have summed up the ladder-type diagram in the particle-hole channel, only to obtain Eq. (82). The coefficients β_j appearing in Eq. (82) are expressed in terms of F_0 and F_5, by way of Eqs. (84)–(91) and Eq. (78). When the self-consistent Born (scB) solution is used for F_0 and F_5, at least one of these β_j is expected to have a diffusion pole structure. On the one hand, none of a_j defined in Eq. (78) does not diverge at $\omega=0$. As such, some of f_j^{-1} should be zero at $\omega=0$. In this section, we will identify which f_j diverges at small ω. This also determines the asymptotic *tensor* form of the diffuson in the small ω limit.

To do this, let us first start from the self-consistent Born equations of F_0 and F_5, i.e., Equations (38)–(41), or equivalently, begin with the following two:

$$(F_0 - F_5) - \alpha\sum_k \frac{(F_0 + F_5)}{k^2 - (F_0^2 - F_5^2)} = \mu - m + i\delta, \tag{92}$$

$$(F_0 + F_5) - \alpha\sum_k \frac{(F_0 - F_5)}{k^2 - (F_0^2 - F_5^2)} = \mu + m + i\delta. \tag{93}$$

Then, subtracting Eqs. (92) and (93) by their respective complex conjugates, we can readily obtain

$$\begin{bmatrix} a_{04} - a_{23} & 3a_1 \\ 3a_1 & a_{04} + a_{23}\end{bmatrix}_{|\omega=0}\begin{bmatrix} F_0'' - F_5'' \\ F_0'' + F_5''\end{bmatrix} = \begin{bmatrix} 0\\ 0\end{bmatrix}, \tag{94}$$

where Eq. (87) and Eq. (78) were used. This equation indicates that the determinant of the 2×2 matrix in the left-hand side should be zero, provided that either F_0'' or F_5'' is nonzero. Any compressible phase having a finite density of state supports $F_0''^2 + F_5''^2 \neq 0$. As such, any scB solution in the compressible phase always guarantees the following identity:

$$\{9a_1^2 - a_{04}^2 + a_{23}^2\}_{|\omega=0} \equiv 0. \tag{95}$$

Since a_1 defined in Eq. (78) is negative definite at $\omega=0$, more accurately, Eq. (95) should be replaced by

$$3a_{1|\omega=0} = -\{\sqrt{a_{04}^2 - a_{23}^2}\}|_{\omega=0}. \tag{96}$$

Observing Eq. (91), notice that this is actually identical to the following:

$$\{f_4^{-1}\}_{|\omega=0} \equiv 0. \tag{97}$$

Namely, f_4 carries the diffusion pole.

f_1, f_2, and f_3 generally cannot have any pole structure for the small ω region. To see this explicitly, note first that when generalized into the finite q case, f_4 takes the following asymptotic form:

$$f_4(\omega) \simeq \frac{1}{a_0}\frac{1}{\tau i\omega} \to f_4(q,\omega) \simeq \frac{1}{a_0}\frac{1}{\tau i\omega - D_0 q^2}. \tag{98}$$

In the right-hand side, we have replaced $i\omega$ by $i\omega - D_0 q^2$ with the bare diffusion constant D_0. By retaining the subleading contribution in small q appearing in Eq. (73), one can explicitly calculate its leading-order expression in the large $\bar{\mu}\tau$ limit,

$$D_0 \equiv \frac{1}{6}\frac{\alpha_c - \alpha}{\alpha_c + \alpha}\tau, \tag{99}$$

which is positive definite for $\alpha < \alpha_c$. Similarly, we can obtain the asymptotic form of f_1, f_2, and f_3 at $\omega, q \simeq 0$,

$$f_1 \simeq \frac{1}{a_0}\frac{1}{\tau i\omega - D_1 q^2 - \tau_1^{-1}}, \tag{100}$$

$$f_2 \simeq \frac{1}{a_0}\frac{1}{\tau i\omega - D_2 q^2 - \tau_2^{-1}}, \tag{101}$$

$$f_3 \simeq \frac{1}{a_0}\frac{1}{\tau i\omega - D q^2 - \tau_{\text{topo}}^{-1}}. \tag{102}$$

τ_1^{-1} and τ_2^{-1} above are positive definite,

$$\tau_1^{-1} \equiv \tau_2^{-1} + \tau_{\text{topo}}^{-1} > 0,$$

$$\tau_2^{-1} \equiv \tau^{-1} \times \left\{\frac{8a_1^2}{a_0}\right\}_{|\omega=0} > 0, \tag{103}$$

while τ_{topo}^{-1} being positive semidefinite;

$$\tau_{\text{topo}}^{-1} \equiv \tau^{-1} \times \left\{\frac{4(-a_0 a_4 + a_2 a_3)}{a_0}\right\}_{|\omega=0} \geq 0. \tag{104}$$

The two inequalities in Eq. (103) and Eq. (104) are indeed supported by Eq. (79) and Eqs. (79) and (80), respectively. These expressions indicate that f_1, f_2, and f_3 always experience the infrared cutoff for the low-energy and long-wavelength region.

Comparing Eq. (104) with Eq. (81), notice also that τ_{topo}^{-1} reduces to zero in the massless case, $\tau_{\text{topo}}^{-1} \propto m^2$, since a_2, a_3, and a_4 being zero. As such, f_3 acquires a same diffusion pole as f_4 does in the absence of the topological mass. Meanwhile f_1 and f_2 always suffer from the (relatively large) finite infrared cutoff τ_2^{-1}, irrespectively of the topological mass term. Thus, we will retain in Eq. (84) only those terms proportional to f_3 and f_4. Based on the same spirit, we will also replace Eq. (85) by its leading-order contribution in small ω and q,

$$\beta_{11} \simeq \frac{3a_1}{8}(-f_3 + f_4), \tag{105}$$

and use the following asymptotic expressions for $\{\beta_0, \cdots, \beta_{11}\}$,

$$\{\beta_0, \beta_4, \beta_5, \beta_{10}\} \simeq \frac{\delta a_{04|\omega=0}}{8} f_3\{-1,1,-1,1\} - \frac{a_{04|\omega=0}}{8} f_4\{1,1,1,1\},$$

$$\{\beta_1, \beta_6, \beta_7, \beta_{11}\} \simeq \frac{3a_{1|\omega=0}}{8} f_3\{1,1,-1,-1\} + \frac{3a_{1|\omega=0}}{8} f_4\{1,1,1,1\},$$

$$\{\beta_2, \beta_3, \beta_8, \beta_9\} \simeq \frac{\delta a_{23|\omega=0}}{8} f_3\{1,-1,1,-1\} + \frac{a_{23|\omega=0}}{8} f_4\{1,1,1,1\}.$$

With these equations, the asymptotic form of the diffuson in small ω and q will be derived out of Eq. (82). It consists of the two *quasi*degenerate dominant contributions,

$$\hat{\Gamma}^d(q,\omega) \simeq \frac{f_4}{8}\hat{\Gamma}_1^d + \frac{f_3}{8}\hat{\Gamma}_2^d, \tag{106}$$

where the two ω-, q-free tensors are given as follows:

$$\hat{\Gamma}_1^d \equiv [-a_{04} \quad 3a_1 \quad a_{23}]_{|\omega=0} \cdot \begin{bmatrix} (\hat{1}+\hat{T}_4)\cdot(\hat{1}+\hat{S}_1) \\ (\hat{1}+\hat{T}_4)\cdot(\hat{T}_1+\hat{S}_2) \\ (\hat{T}_2+\hat{T}_3)\cdot(\hat{1}+\hat{S}_1) \end{bmatrix}, \tag{107}$$

$$\hat{\Gamma}_2^d \equiv [-\delta a_{04} \quad 3a_1 \quad \delta a_{23}]_{|\omega=0} \cdot \begin{bmatrix} (\hat{1}-\hat{T}_4)\cdot(\hat{1}+\hat{S}_1) \\ (\hat{1}-\hat{T}_4)\cdot(\hat{T}_1+\hat{S}_2) \\ (\hat{T}_2-\hat{T}_3)\cdot(\hat{1}+\hat{S}_1) \end{bmatrix}. \tag{108}$$

C. Parity diffusion mode

To capture the physical meanings of the two members in Eq. (106), notice first that in the absence of the topological mass m, our Hamiltonian, i.e., Eq. (5) with the chemical-potential-type disorder, becomes invariant under the following $U(1)$ transformation:

$$e^{i\theta\int\psi^\dagger(r)\hat{\gamma}_{45}\psi(r)}\cdot\hat{\mathcal{H}}\cdot e^{-i\theta\int\psi^\dagger(r)\hat{\gamma}_{45}\psi(r)}=\hat{\mathcal{H}}, \tag{109}$$

irrespectively of the strength of the disorder. As a result, each ensemble at $m=0$ acquires another conserved charge, $\psi^\dagger(r)\hat{\gamma}_{45}\psi(r)$, which is the parity-density degree of freedom (DOF) (see Table II). Observing this $U(1)$ symmetry, we can then expect that the diffuson $\hat{\Gamma}^d(q,\omega)$ calculated above should consist of two diffusive modes at $m=0$: One describes the usual charge diffusion and the other is for the diffusion of this parity density. These two physical modes actually correspond to the first term and the second term in Eq. (106). In fact, the parity density becomes nonconserved in the presence of finite m, which is consistent with the finite infrared cutoff $\tau_{\text{topo}}^{-1}\propto m^2$ appearing only in f_3 [see Eqs. (102) and (98)].

To uphold this consideration more directly, one can also calculate the density correlation function and parity-density correlation function at $m=0$,

$$\phi_0(q,\omega)\equiv\sum_{k,k',\alpha,\beta}\Phi_{\alpha\beta,\beta\alpha}(k,k';q,\omega),$$

$$\phi'_{45}(q,\omega)\equiv\sum_{\cdots}[\hat{\gamma}_{45}]_{\beta\alpha}\Phi_{\alpha\delta,\gamma\beta}(k,k';q,\omega)[\hat{\gamma}_{45}]_{\delta\gamma},$$

where $\hat{\Phi}(k,k';q,\omega)$ stands for the response function [see Eq. (B2) for its definition]. By noting that this response function for small q and ω is dominated by the diffuson,

$$\begin{aligned}\Phi_{\alpha\delta,\gamma\beta}(k,k';q,\omega)\simeq&-\frac{\alpha}{2\pi i}\hat{G}^R_{\alpha\alpha_1}(k_+,\mu_+)\hat{G}^A_{\beta_1\beta}(k_-,\mu_-)\\&\times[\hat{\Gamma}^d(q,\omega)]_{\alpha_1\delta_1,\gamma_1\beta_1}\hat{G}^R_{\delta_1\delta}(k'_+,\mu_+)\\&\times\hat{G}^A_{\gamma\gamma_1}(k'_-,\mu_-),\end{aligned} \tag{110}$$

one can explicitly see that the two terms appearing in Eq. (106) actually contribute the density correlation and parity-density correlation separately,

$$\{\phi_0(q,\omega),\phi'_{45}(q,\omega)\}\simeq-\frac{8ia_0}{\alpha}\{f_4,f_3\}. \tag{111}$$

D. Cooperon and the quantum conductivity correction

When the hole lines being time reversed, Eq. (106) will be transcribed into the two quasidegenerate dominant contributions to the series sum of the fan-type diagrams [see Fig. 11(b)],

$$\hat{U}^{\text{coop}}(k+k',\omega)=\frac{\alpha}{8}\{f_4\hat{U}^{\text{c}}_1+f_3\hat{U}^{\text{c}}_2\}_{|q\to k+k'}, \tag{112}$$

where the ω-, q-free tensors $\hat{U}^{\text{c}}_{1,2}$ are derived out of Eqs. (107) and (108), respectively,

$$\hat{U}^{\text{c}}_1\equiv[-a_{04}\quad 3a_1\quad a_{23}]_{|\omega=0}\cdot\begin{bmatrix}(\hat{1}+\hat{T}_4)\cdot(\hat{1}-\hat{S}_1)\\(\hat{1}-\hat{T}_4)\cdot(-\hat{T}_1+\hat{S}_2)\\(\hat{T}_2+\hat{T}_3)\cdot(\hat{1}-\hat{S}_1)\end{bmatrix}, \tag{113}$$

$$\hat{U}^{\text{c}}_2\equiv[-\delta a_{04}\quad 3a_1\quad \delta a_{23}]_{|\omega=0}\cdot\begin{bmatrix}(\hat{1}-\hat{T}_4)\cdot(\hat{1}-\hat{S}_1)\\(\hat{1}+\hat{T}_4)\cdot(-\hat{T}_1+\hat{S}_2)\\(\hat{T}_2-\hat{T}_3)\cdot(\hat{1}-\hat{S}_1)\end{bmatrix}. \tag{114}$$

Substituting these two Cooperon terms into the current-current correlation function, we can explicitly show that the two members in Eq. (112) lead the same magnitude of the anti-weak-localization (AWL) behavior at the critical point ($m=0$),

$$\begin{aligned}&\sum_{L^{-1}<|k+k'|<l^{-1}}\frac{\alpha f_4}{8}\sum_k\{\hat{G}^A(k,\mu)\cdot\hat{\gamma}_1\cdot\hat{G}^R(k,\mu)\}_{\delta\alpha}\hat{U}^{\text{c}}_{1,\alpha\beta,\gamma\delta}\{\hat{G}^R(-k,\mu)\cdot\hat{\gamma}_1\cdot\hat{G}^A(-k,\mu)\}_{\beta\gamma}\\&=\sum_{\cdots}\frac{\alpha f_4}{8}\sum_k\{\hat{G}^A(k,\mu)\cdot\hat{\gamma}_1\cdot\hat{G}^R(k,\mu)\}_{\delta\alpha}\hat{U}^{\text{c}}_{2,\alpha\beta,\gamma\delta}\{\hat{G}^R(-k,\mu)\cdot\hat{\gamma}_1\cdot\hat{G}^A(-k,\mu)\}_{\beta\gamma}\\&=\frac{\alpha}{8}\frac{1}{D_0\tau}\sum_{\cdots}\frac{1}{(k+k')^2}\sum_k\{\hat{G}^A(k,\mu)\cdot\hat{\gamma}_1\cdot\hat{G}^R(k,\mu)\}_{\delta\alpha}\{\hat{1}-\hat{S}_1-\hat{T}_1+\hat{S}_2\}_{\alpha\beta,\gamma\delta}\{\hat{G}^R(-k,\mu)\cdot\hat{\gamma}_1\cdot\hat{G}^A(-k,\mu)\}_{\beta\gamma}\\&=c(l^{-1}-L^{-1})\end{aligned} \tag{115}$$

with $c=16\pi\cdot(1+\frac{\alpha}{\alpha_c})$ being positive definite. [We used $a_2=a_3=a_4=0$ and $-3a_1=a_0$ in Eqs. (113) and (114)]. When the finite topological mass m is introduced, however, the second member of Eq. (112) becomes suppressed since the infrared divergence of f_3 becomes truncated by finite τ_{topo}^{-1}. As a result, one half of the AWL correction becomes ineffective in the presence of finite m (quantum correction doubling).

V. DISCUSSION

A. Summary of our findings

In this paper, we have studied the effects of the time-reversal invariant disorder on the quantum spin Hall system.[25–29] We have especially focused on the quantum critical point (QCP) which intervenes the 3D topological insulator (TI) and a 3D ordinary insulator. The topological insulator supports a single 2+1 massless surface Dirac fermion for each boundary, while an ordinary insulator does not have any. As such, the bulk-wave function in those parameter regions (or point), which intervene these two insulating phases, should be extended so as to mediate two opposite surfaces. Such extended bulk states are stable against $\mathcal{T}$-invariant disorders, as far as each surface state in the TI phase is stable. In fact, Nomura *et al.*[30] and Bardarson *et al.*[31] recently calculated the β function numerically, and demonstrated that the single copy of the 2+1 massless Dirac fermion is topologically stable against the $\mathcal{T}$-invariant disorders. This observation strongly indicates that there *always* exists delocalized (bulk-critical) region between the 3D topological insulator phase and a 3D ordinary insulator phase.

To uncover the nature of this peculiar quantum critical point (or region), we have studied the disorder effect on its minimal model, i.e., single 3+1 Dirac fermion. As a basis for this, we first studied in Sec. III how the chemical-potential-type disorder brings about a finite lifetime of the zero-energy wave function. We then observed that there exists a certain critical disorder strength, above which the DOS at the zero energy becomes finite [see Eq. (51)].

When the finite topological mass is introduced, a system eventually enters either the TI or an ordinary insulator, depending on the sign of the topological mass. In Sec. III, we studied how this topological mass is renormalized by the chemical-potential-type disorder within the self-consistent Born approximation. By doing this, we have determined the phase boundary between the compressible phase and the gapped phase (see Figs. 9 and 10).

To further infer the low-energy structure in this compressible phase, we have derived in Sec. IV the diffuson, Cooperon, and the weak-localization (WL) correction to the electric conductivity. We then observed that the charge diffusion mode and parity diffusion mode dominate the diffuson [see Eq. (106)]; the charge channel always carries the diffusion pole structure, while the parity-density channel becomes massless only in the absence of the topological mass. In the presence of the finite topological mass m, it generally suffers from the infrared cutoff $\tau_{\text{topo}}^{-1}\propto m^2$.

Corresponding to this feature in the diffuson, the Cooperon is also composed of two quasidegenerate dominant contributions [see Eqs. (112)–(114)]. In the zero topological mass limit, these two contributions bring about the same magnitude of the anti-weak-localization (AWL) correction with each other. When the finite topological mass m is introduced, however, that from the parity-density channel becomes truncated by the finite infrared cutoff τ_{topo}^{-1}. As such, one half of the AWL correction becomes ineffective. As a result, on increasing m, the AWL correction exhibits a crossover into *one half* of its original value (quantum correction doubling).

B. Levitation and pair-annihilation phenomena

Let us discuss open issues in the 3D Z_2 QSH system in the viewpoint of our findings. As a tightly related topic to the stability of the QCP, the levitation and pair-annihilations phenomena of the extended states[32] were recently observed in the 2D Z_2 quantum spin Hall systems by Onoda *et al.*[25] They numerically studied the disorder effect on the Kane-Mele model[5] on the honeycomb lattice. In the clean case the system is set to be in the QSHI phase; namely, the spectrum consists of two bands, and there is a gap between them. When the system is disordered, some states far from the band centers become localized, while there are energy regions of delocalized states, located at the centers of the upper (empty) band and lower (filled) band. What Onoda *et al.*[25] found is that each of these two does not disappear *by itself* when the disorder strength is increased. Instead, when the disorder becomes much stronger than the disorder strength for the localization in an ordinary insulator, these two merge into one bundle of extended states energetically, and annihilate in pair [see Fig. 12(a)].

To argue this phenomenon more generally, consider the three-dimensional parameter space spanned by the topological mass term m, chemical potential μ, and disorder strength α. From the surface-state arguments described in Sec. I, two insulating phases having different types of edge (surface) states, i.e., the topological insulator and an ordinary insulator, should be disconnected by the delocalized (bulk-critical) region. Then, when a finite topological mass term m changes its sign from positive (topological insulator side) to negative (ordinary insulator side), we should also expect that a similar levitation and pair-annihilation phenomenon occurs. Namely, when a system transits from the topological insulator side to the ordinary insulator side, the region of extended states in the upper band and that in the lower band always merge and annihilate with each other [see Fig. 12(b)]. Combining this picture with Onoda's numerical observation,[33] one can then expect that the delocalized (bulk-critical) region constitutes a *surface* in the 3D parameter space spanned by μ, m, and α, only to isolate the topological insulator phase from an ordinary insulator phase (see Fig. 13).

C. Possible microscopic scenario

Generally speaking, one has to go beyond our mean-field treatment of disorder in order to study the behaviors of mobility edges. However, we can still speculate the microscopic picture of the levitation and pair-annihilation phenomena dis-

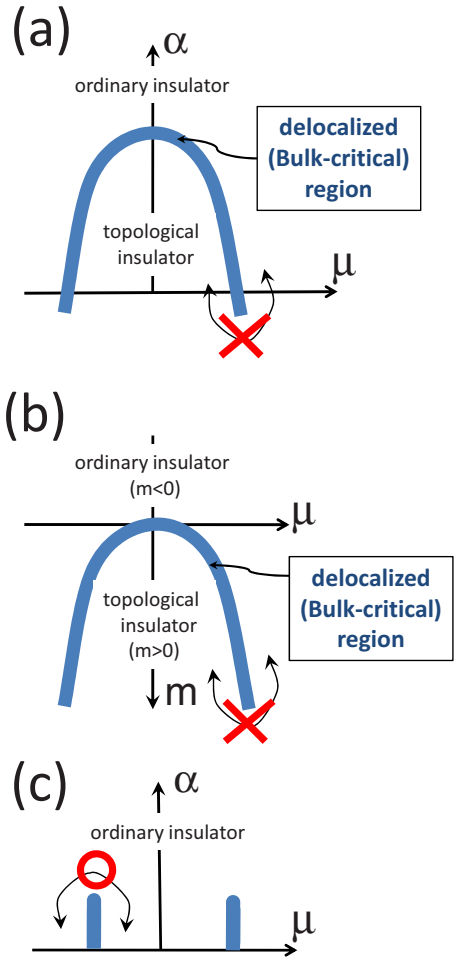

FIG. 12. (Color online) (a) Onoda's phase diagram (Ref. 25) in the α-μ plane with $m>0$ (topological insulator side). (b) A schematic phase diagram in the m-μ plane, which is expected from the surface (edge) state's argument described in Sec. I. (c). A schematic phase diagram in the α-μ plane of the ordinary insulator side ($m<0$). In (a)–(c), we have two delocalized energy regions (blue filled regions), which locate at the center of the upper band and the lower band. In (a), these two delocalized regions eventually merge and annihilate in pair when α increases. As a result, the topological insulator and ordinary insulator are always disconnected by the bulk-critical (delocalized) region. In (c), however, two delocalized regions registered at the upper band and the lower band annihilate without merging each other when α increases. Thus, all the insulating regions appearing in (c) are adiabatically connected from one point to others. In (b), two delocalized regions merge and annihilate with each other, when the topological mass m changes its sign from positive to negative. As a result, the topological insulator and ordinary insulator are again disconnected from each other by the bulk-critical (delocalized) region, as in (a).

cussed above in terms of the quantum correction doubling found in this paper.

We expect that the intervening bulk-critical region [blue filled region in Figs. 12(a) and 12(b) and Fig. 13] corresponds to the $\tau_{\mathrm{topo}}^{-1}\equiv 0$ region. Namely, when a system transits from the topological insulator to an ordinary insulator, we surmise that *one of the high-energy modes, i.e., parity diffusion mode appearing in* Eq. (106)*, becomes massless*

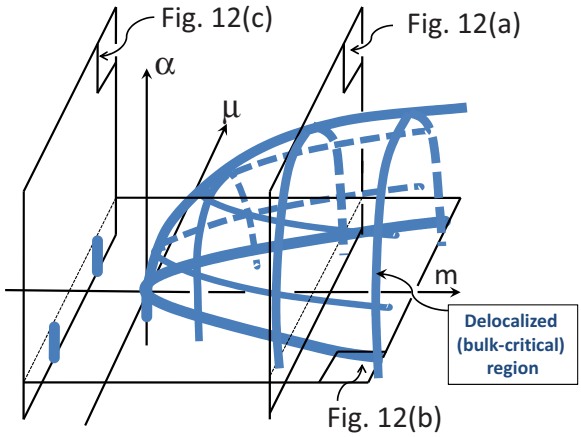

FIG. 13. (Color online) A schematic phase diagram in the α-μ-m space. The vertical axis is the disorder strength α, while the horizontal plane is spanned by the chemical potential μ and the topological mass m. The delocalized region (blue filled region) constitutes a *surface* in this three-dimensional parameter space, so that an ordinary insulator phase and the topological insulator phase are adiabatically *disconnected* from each other. Namely, one cannot move from one phase to the other, without crossing the delocalized region, i.e., bulk-critical region. The phase diagram for the constant positive m (topological insulator side) and that for the constant negative m (ordinary insulator side) are separately described in Figs. 12(a) and 12(c), respectively. The phase diagram for the constant α corresponds to Fig. 12(b).

once, only to guarantee the existence of the bulk-critical region between these two insulating phases. This conjecture naturally leads to the following microscopic scenario of the levitation and pair-annihilation phenomena.

Suppose that the $\mathcal{T}$-symmetric disorder is introduced in the topological insulator. We assume that such disorder potential is strong enough to make the system localized. But it is not strong enough to make the upper (empty) band and low (occupied) band mixed with each other. Namely, a system locates in the topological insulator side of Fig. 13 so that it can be adiabatically connected into the topological insulator phase in the clean limit. In such localized phase, we expect that a parity diffusion mode always exists in the high-energy region and is *protected* by the infrared cutoff $\tau_{\mathrm{topo}}^{-1}$, while the charge diffusion mode disappears because of the relatively strong disorders [see Fig. 14(a)]. Starting from this localized phase, let us decrease the topological mass term (or further increase the disorder strength). Then, this infrared cutoff $\tau_{\mathrm{topo}}^{-1}$ associated with the parity diffusion mode decreases gradually, only to be renormalized to be zero at the transition point [see Fig. 14(b)]. Namely, at this transition point, the parity diffusion mode becomes massless. As a result, the Cooperon term corresponding to this parity diffusion mode, i.e., Eq. (114), becomes effective and brings about the positive quantum interference effect on the back-scattering processes, in the same way as in Sec. IV D. Because of this positive quantum interference effect, which emerges only when the parity diffusion mode becomes massless, the charge diffusion constant recovers at around $\tau_{\mathrm{topo}}^{-1}\simeq 0$, even in the presence of the relatively strong disorder [see the red line in Fig. 14(b)].

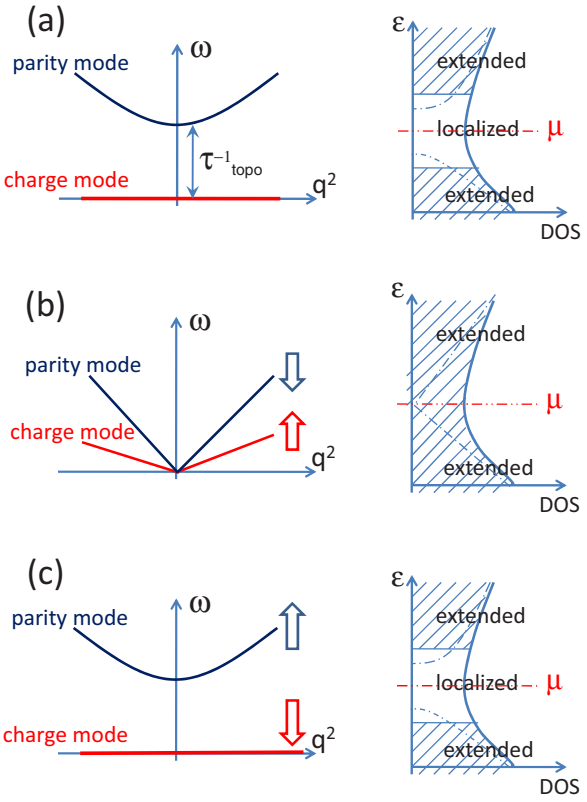

FIG. 14. (Color online) (a) The low-energy spectrum in the topological insulator side contains two relevant diffusion modes. One is the usual charge diffusion mode, which disappears in the presence of relatively strong disorders. The other is the parity diffusion mode, which is protected by the infrared cutoff τ_{topo}^{-1} from the disorders. (b) When a system transits from the topological insulator phase to the ordinary insulator phase, the parity diffusion mode becomes massless. Namely, when one further increases the disorder, starting from (a), τ_{topo}^{-1} becomes renormalized by the disorder, only to reach zero. As a result, the Cooperon term corresponding to this parity diffusion mode becomes effective and induces the positive quantum interference effect on the backward-scattering process of the charge-degrees of freedom. Because of this, the charge diffusion mode recovers at $\tau_{\text{topo}}^{-1}=0$. (c) The low-energy spectrum in the ordinary insulator side.

However, when one further decreases the topological mass (or increases the disorder strength), the infrared cutoff τ_{topo}^{-1} becomes finite again. As a result, this positive quantum interference effect due to the massless parity diffusion mode becomes ineffective again, only to lead a system into an insulating phase [see Fig. 14(c)]. This insulating phase is now adiabatically connected to an ordinary insulator in the clean limit.

To uphold this microscopic picture, we need to consider several ingredients missing in our approach.[34] We will enumerate them in the following. As indicated in Figs. 12 and 13, the pair annihilation occurs only in the topological insulator side. Namely, the phase diagram is *asymmetric* with respect to the sign change in the topological mass term. On the other hand, all the findings in this paper are symmetric with respect to the sign change in this mass term. This is obviously because our starting model is the effective continuum model, describing only the *local* structure around a certain k point. On the other hand, the Z_2 topological number is determined from the *global* information of the Bloch wave functions' phase in the k space.[15] Therefore, in such an effective continuum model one cannot determine whether the topological insulator *by itself* corresponds to the $m>0$ phase or the $m<0$ phase. Instead, it simply dictates that one of these two should be the topological insulator, and the other is an ordinary insulator. As such, to describe the asymmetric behavior of the mobility edge as in Fig. 13, we clearly have to deal with lattice models.

In the present work we treated disorder in the mean-field level, considering only the Cooperon correction. To verify the aforementioned scenario, we thus also need to deal with interactions among the various low-energy modes, beyond the mean-field treatment. In such situations, the intermode interaction between the quasidegenerate Goldstone modes found in Sec. IV certainly plays an important role in the levitation and pair-annihilation phenomena.

ACKNOWLEDGMENTS

We are grateful to Leon Balents, A. P. Schnyder, K-i Imura, Kentaro Nomura, Shinsei Ryu, Hideaki Obuse, Akira Furusaki, and Hiroshi Kohno for helpful discussions. This research was supported in part by Grant-in-Aids for Creative Scientific Research (15GS0213) from the Ministry of Education, Culture, Sports, Science and Technology of Japan. R.S. was financially supported previously by Osaka University and currently by the Institute of Physical and Chemical Research (RIKEN). Part of this work was done during the ISSP-YITP joint-workshop entitled "Topological Aspects of Solid State Physics (TASSP)."

APPENDIX A: EFFECTS OF GENERIC TIME-REVERSAL INVARIANT DISORDERS

In this paper, we have restricted ourselves to the chemical-potential-type disorder for simplicity. However, there exist in general several other types of $\mathcal{T}$-invariant disorder potentials, as described in Sec. II [see Eq. (7)]. We basically expect that these additional time-reversal invariant disorders will not change our results drastically. To uphold this expectation, we study in this appendix how our self-consistent Born solution is modified in the presence of generic time-reversal invariant disorders, focusing on the zero-energy wave function at the critical point. As a result, we will obtain the following facts, which partially support this expectation. One is that, when only the diagonal correlations, Δ_{jj}, are present, our solutions derived in Sec. III do not change at all [see Eqs. (A16), (A4), and (A8)]. When the off-diagonal correlation such as Δ_{05} is introduced, F_5 acquires a finite imaginary part, i.e., $F_5'' \neq 0$, even at the zero-energy state at the critical point [see Eqs. (A16), (A4), and (A8)]. However, provided that Δ_{05} is not so large in comparison with the diagonal correlation such as Δ_{00}, Δ_{55}, etc., the effect of the nonzero F_5'' is expected to be negligible.

The generic $\mathcal{T}$ invariant disorders bring about the coupling between F_5 and F_0 more explicitly in the self-consistent

Born (scB) equation. Namely, instead of Eqs. (38) and (39), our scB equation reads

$$\int_{0<|k|<1} d^3k \frac{A_+F_0 - BF_5}{F_0^2 - \sum_{\mu=1}^{5} F_\mu^2} = f_0 - F_0, \tag{A1}$$

$$\int_{0<|k|<1} d^3k \frac{BF_0 - A_-F_5}{F_0^2 - \sum_{\mu=1}^{5} F_\mu^2} = f_5 - F_5, \tag{A2}$$

where only the following three parameters are the relevant model parameters:

$$A_\pm \equiv \left\{ \Delta_{00} + \Delta_{55} \pm \sum_{j\in\{15,\cdots,45\}} \Delta_{jj} \right\} \Lambda, \tag{A3}$$

$$B \equiv 2\Delta_{05}\Lambda. \tag{A4}$$

The coefficients of $\hat{\gamma}_{1,2,3,4}$ in the one-point Green's function, on the other hand, are again free from renormalization,

$$F_{1,2,3} \equiv f_{1,2,3} = -k_{1,2,3}, \quad F_4 \equiv f_4 \equiv 0. \tag{A5}$$

In terms of G defined in Eqs. (40) and (41), we can rewrite Eqs. (A1) and (A2) more transparently,

$$\begin{cases} 2\pi(A_+F_0 - BF_5)\cdot G = f_0 - F_0, \\ 2\pi(BF_0 - A_-F_5)\cdot G = f_5 - F_5. \end{cases} \tag{A6}$$

When it comes to the zero-energy wave function at the critical point, i.e., $f_0=f_5=0$, this coupled equation could be "diagonalized,"

$$(1 - \eta_\sigma G)(\lambda_\sigma F_0 - F_5) = 0, \tag{A7}$$

with $\sigma=\pm$. η_σ and λ_σ are defined as follows:

$$\lambda_\pm \equiv \frac{1}{B}(\Delta_s \pm \sqrt{\Delta_s^2 - B^2}), \tag{A8}$$

$$\eta_\pm \equiv -(\Delta_a \pm \sqrt{\Delta_s^2 - B^2}), \tag{A9}$$

with positive definite Δ_s and Δ_a,

$$\Delta_s \equiv \frac{1}{2}(A_+ + A_-) = \Delta_{00}\Lambda + \Delta_{55}\Lambda,$$

$$\Delta_a \equiv \frac{1}{2}(A_+ - A_-) = \sum_{j\in\{15,\cdots,45\}} \Delta_{jj}\Lambda.$$

Observing Eqs. (17), note also that Δ_s defined above is always greater than $|B|$ defined in Eq. (A4),

$$\Delta_s^2 - B^2 > 0. \tag{A10}$$

Equation (A7) with $\sigma=\pm$ can be trivially satisfied by $F_0=F_5\equiv 0$. In what follows, we will enumerate all possible nontrivial solutions of this coupled equation. Let us first write down the real part and imaginary part of Eq. (A7) for both $\sigma=\pm$, separately. Noting that $\lambda_\pm$ and $\eta_\pm$ are real valued, we have the following for $\sigma=+$:

$$\begin{bmatrix} 1-\eta_+ \mathrm{Re}\, G & \eta_+ \mathrm{Im}\, G \\ -\eta_+ \mathrm{Im}\, G & 1-\eta_+ \mathrm{Re}\, G \end{bmatrix} \begin{bmatrix} \lambda_+F_0' - F_5' \\ \lambda_+F_0'' - F_5'' \end{bmatrix} = 0. \tag{A11}$$

For $\sigma=-$, we have

$$\begin{bmatrix} 1-\eta_- \mathrm{Re}\, G & \eta_- \mathrm{Im}\, G \\ -\eta_- \mathrm{Im}\, G & 1-\eta_- \mathrm{Re}\, G \end{bmatrix} \begin{bmatrix} \lambda_-F_0' - F_5' \\ \lambda_-F_0'' - F_5'' \end{bmatrix} = 0. \tag{A12}$$

Observing Eq. (A10), notice that $\lambda_+ \neq \lambda_-$ in general. As such, (F_0, F_5) cannot satisfy $F_5=\lambda_-F_0$ and $F_5=\lambda_+F_0$ *simultaneously*. Thus, when $F_5=\lambda_-F_0$ is adopted, the determinant of the 2×2 matrix in Eq. (A11) should be zero,

$$\begin{vmatrix} 1-\eta_+ \mathrm{Re}\, G & \eta_+ \mathrm{Im}\, G \\ -\eta_+ \mathrm{Im}\, G & 1-\eta_+ \mathrm{Re}\, G \end{vmatrix} = 0, \tag{A13}$$

or equivalently

$$1 = \eta_+ \mathrm{Re}\, G, \quad \mathrm{Im}\, G = 0.$$

On the other hand, when $F_5=\lambda_+F_0$ holds true, we have the following in turn:

$$1 = \eta_- \mathrm{Re}\, G, \quad \mathrm{Im}\, G = 0.$$

We thus have the only two possible nontrivial solutions,

$$\begin{cases} \text{(Bi)}: F_5 = \lambda_-F_0, & 1 = \eta_+ \mathrm{Re}\, G \ \text{ and } \ \mathrm{Im}\, G = 0, \\ \text{(Bii)}: F_5 = \lambda_+F_0, & 1 = \eta_- \mathrm{Re}\, G \ \text{ and } \ \mathrm{Im}\, G = 0. \end{cases}$$

In either case, $\mathrm{Im}\, G=0$ readily leads us to $a=0$ first. The reasoning of this was already described in Sec. III A 1. When $a=0$, the real part of the function G becomes simplified; $\mathrm{Re}\, G_{|a=0} \equiv -2+2b \arctan[b^{-1}]$ [see Eq. (43)]. Thus, above two solutions will be transcribed into the following two:

$$b \arctan[b^{-1}] = \frac{1+2\eta_\mp}{2\eta_\mp}, \tag{A14}$$

with $F_5=\lambda_\pm F_0$, respectively.

Since the left-hand side of Eq. (A14) is positive semidefinite, we have the following two parameter region supporting nontrivial solutions:

$$\begin{cases} (a): & \eta_+ < -\frac{1}{2} < \eta_-, \\ (b): & \eta_+ < \eta_- < -\frac{1}{2}. \end{cases}$$

We also used $\eta_- > \eta_+$, which is trivially supported by Eq. (A10). These two parameter regions are depicted in Fig. 15, where region (a) actually includes the "compressible phase" argued in Secs. III and IV, i.e., $\alpha > \alpha_c$ and $B=\Delta_a=0$.

In region (a), only the type-(Bi) solution becomes possible,

$$F_5 = \lambda_-F_0, \ (a,b) \simeq \left(0, \frac{\pi + 2\pi\eta_+}{4\eta_+}\right). \tag{A15}$$

Under $F_0^2 - F_5^2 \equiv (a+ib)^2$, this is identical to the following solution:

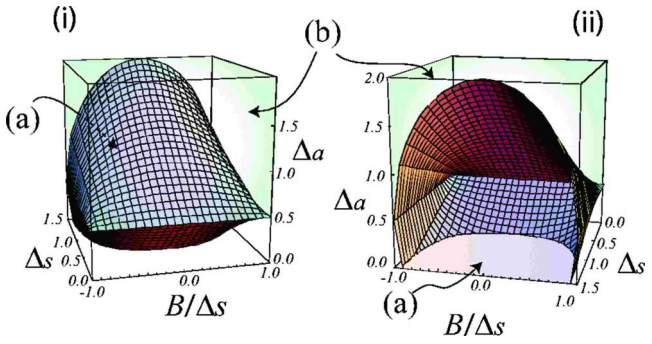

FIG. 15. (Color online) The phase diagram of the scB solution in the presence of generic time-reversal invariant disorders. Region (a) includes the "compressible phase" argued in Secs. III and IV, i.e., $\alpha > \alpha_c$ at $B=\Delta_a=0$. Region (b) appears only when $\Delta_a \equiv \Sigma_{j=\{15,25,\cdots,45\}}\Delta_{jj} > 0.5$. Note also that $\Delta_a, \Delta_s > 0$ and $B < \Delta_s$ because of Eq. (17) [see also Eq. (A10)].

$$(F_0, F_5) = \pm i \frac{|b|}{\sqrt{1-\lambda_-^2}}(1, \lambda_-). \tag{A16}$$

This solution comprises continuously with the physical scB solution described in Sec. III. Namely, when Δ_a taken to be zero, Eq. (A16) precisely reduces to Eq. (51).

When it comes to the region-(b), type-(Bii) also becomes a possible solution,

$$F_5 = \lambda_+ F_0, \ (a,b) \simeq \left(0, \frac{\pi + 2\pi\eta_-}{4\eta_-}\right), \tag{A17}$$

namely,

$$(F_0, F_5) = \mp \frac{|b|}{\sqrt{\lambda_+^{-2}-1}}(\lambda_+^{-1}, 1). \tag{A18}$$

In the absence of finite B and Δ_a, however, this solution is continued into Eq. (49). Thus, this can never hold true therein. Because of this, we judge the type-(Bii) solution to be unphysical.

APPENDIX B: MODE-MODE COUPLING THEORY

The weak-localization calculation (and also the self-consistent Born calculation) described in Sec. IV has the small coupling constant $1/(\mu\tau)$ only for the weakly disordered region, i.e., $\alpha < \alpha_c$, while it becomes an uncontrolled analysis for $\alpha > \alpha_c$. Bearing in mind this strong disorder region, we will employ in this appendix more phenomenological calculations, based on the mode-mode coupling theory.[35] Without resorting to the Kubo formula, this theoretical framework gives us a mean-field equation for the diffusion constant D, where the quantum correction due to the Cooperon term is taken into account as in the standard weak-localization calculation.[35] The final results of this appendix such as Eqs. (B54) and (B61) indicate that this quantum correction becomes doubled, when the topological mass term m is fined tuned to be zero.

The calculation consists of two steps. The first step begins with the Bethe-Salpeter (BS) equation for the response function $\Phi_{\alpha\delta,\gamma\beta}(k,k';q,\omega)$,

$$\Phi_{\alpha\delta,\gamma\beta}(k,k';q,\omega) = G^R_{\alpha\alpha_1}(k_+,\mu_+)G^A_{\beta_1\beta}(k_-,\mu_-)\left\{-\frac{1}{2\pi i}\delta_{\alpha_1\delta}\delta_{\gamma\beta_1}\delta_{k,k'} + \sum_{k_1} U^{\text{2PIR}}_{\alpha_1\delta_1,\gamma_1\beta_1}(k,k_1;q,\omega)\Phi_{\delta_1\delta,\gamma\gamma_1}(k_1,k';q,\omega)\right\}, \tag{B1}$$

$$\Phi_{\alpha\delta,\gamma\beta}(k,k';q,\omega) \equiv -\frac{1}{2\pi i}\langle G^R_{\alpha\delta}(k_+,k'_+,\mu_+)G^A_{\gamma\beta}(k'_-,k_-,\mu_-)\rangle_{\text{imp}}, \tag{B2}$$

with $k_\pm \equiv k \pm \frac{q}{2}$ and $\mu_\pm \equiv \mu \pm \frac{\omega}{2}$. Out of this equation, we first derive the linearized equations of motion (EOMs) for the density relaxation function $\phi_0(q,\omega)$, current relaxation function $\phi_j(q,\omega)$, and relaxation functions associated with other internal degrees of freedom,

$$\phi_0(q,\omega) \equiv \sum_{k,k'}\sum_{\alpha,\beta,\gamma}[\hat{\gamma}_0]_{\beta\alpha}\Phi_{\alpha\gamma,\gamma\beta}(k,k';q,\omega), \tag{B3}$$

$$\phi_j(q,\omega) \equiv \sum_{k,k'}\sum_{\alpha,\beta,\gamma}\hat{q}_\mu[\hat{\gamma}_\mu]_{\beta\alpha}\Phi_{\alpha\gamma,\gamma\beta}(k,k';q,\omega), \tag{B4}$$

with $\hat{q}$ normalized to be a unit vector. Since the EOMs thus derived are linearized, one can solve them for these relaxation functions, only to obtain their asymptotic expressions for the small q, ω,

$$\phi_0(q,\omega) \sim \frac{1}{\omega + iDq^2}, \quad \phi_j(q,\omega) \sim \frac{q}{\omega + iDq^2}, \ldots. \tag{B5}$$

By way of this, the diffusion constant D appearing in the denominators will be expressed in terms of the *relaxation kernels* $\mathcal{M}_{a,b}(q,\omega)$, latter of which are defined by the *two-particle irreducible* (2PIR) vertex function $\hat{U}^{\text{2PIR}}$ [step (i)],

$$D \equiv i\left\{\frac{\mathcal{M}_{5j,5j}}{\mathcal{M}_{j,j}\mathcal{M}_{5j,5j} - \mathcal{M}_{5j,j}\mathcal{M}_{j,5j}}\right\}_{|q,\omega\equiv 0}. \tag{B6}$$

$$\mathcal{M}_{a,b}(q,\omega) \equiv 2i\tau^{-1}\delta_{ab} + \frac{1}{2^4\pi} \times \sum_{k,k'}[\gamma^{\text{L}}_a(k;q,\omega)]_{\beta\alpha}U^{\text{2PIR}}_{\alpha\delta,\gamma\beta}(k,k';q,\omega) \times [\gamma^{\text{R}}_b(k';q,\omega)]_{\delta\gamma} \tag{B7}$$

[see also Eqs. (B31) and (B32) for the definitions of $\hat{\gamma}^{\text{L,R}}_a$].

The second step begins with the observation that the 2PIR vertex function $\hat{U}^{\text{2PIR}}(k,k';q,\omega)$ in disordered media is usually dominated by the Cooperon at small ω and $k+k'$. The Cooperon is the series sum of the ladder-type diagrams in the particle-particle channel, which is therefore obtained from the diffuson with the hole line time reversed. The diffuson is in turn responsible for the diffusion pole in the relaxation functions, i.e., the denominators in Eq. (B5). As such, in the

presence of the $\mathcal{T}$ symmetry, the asymptotic form of the Cooperon at small ω and $k+k'$ *should* be characterized by the *same* diffusion constant as that in Eq. (B5). Based on this spirit, we will replace the 2PIR vertex function in Eq. (B7) by this asymptotic form of the Cooperon. Through this approximation, Eqs. (B6) and (B7) constitute a *self-consistent equation* for the diffusion constant D [step (ii)].

Irrespective of the magnitude of α, the diffuson consists of the charge diffusion mode and parity diffusion mode,

$$\hat{\Gamma}^d(q,\omega) \propto \frac{1}{\omega + iDq^2}\hat{\Gamma}_1^d + \frac{1}{\omega + iDq^2 + i\tau_{\rm topo}^{-1}}\hat{\Gamma}_2^d, \quad \text{(B8)}$$

with the positive semidefinite $\tau_{\rm topo}^{-1}$ proportional to m^2 [see Eqs. (104), (107), and (108)]. Namely, the second term, i.e., the parity diffusion mode, generally suffers from the *finite* infrared cutoff in the presence of the topological mass, while both of these two equally dominate the low-energy region for $m \simeq 0$,

$$\hat{\Gamma}^d(q,\omega) \propto \begin{cases} \dfrac{1}{\omega + iDq^2}(\hat{\Gamma}_1^d + \hat{\Gamma}_2^d) & \text{for } Dl^{-2} \geq \tau_{\rm topo}^{-1}, \\ \dfrac{1}{\omega + iDq^2}\hat{\Gamma}_1^d & \text{for } Dl^{-2} \leq \tau_{\rm topo}^{-1} \end{cases} \quad \text{(B9)}$$

[see Eqs. (102), (98), and (106)]. In the presence of the $\mathcal{T}$ symmetry, this crossover behavior will be transcribed onto the Cooperon term; the backward-scattering process originated from the parity diffusion mode becomes ineffective, in the presence of the relatively large topological mass m,

$$\hat{U}^{\rm coop}(k+k',\omega) \propto \begin{cases} \dfrac{1}{\omega + iD(k+k')^2}(\hat{U}_1^c + \hat{U}_2^c) & \text{for } Dl^{-2} \geq \tau_{\rm topo}^{-1}, \\ \dfrac{1}{\omega + iD(k+k')^2}\hat{U}_1^c & \text{for } Dl^{-2} \leq \tau_{\rm topo}^{-1} \end{cases}$$

[see Eq. (112)].

Corresponding to these two-mode features, we will derive in this appendix the two limiting gap equations; one is valid for $Dl^{-2} \geq \tau_{\rm topo}^{-1}$, while the other is for $Dl^{-2} \leq \tau_{\rm topo}^{-1}$. This appendix is organized as follows. Appendix B 1 is devoted for step (i), in which the linearized coupled EOMs for the relaxation functions and Eqs. (B6) and (B7) will be derived. Using Eqs. (B6) and (B7), we will derive in Appendix B 2 the gap equations for the two-limiting cases [step (ii)]. By solving these gap equations, we will finally see how the diffusion constant for $\alpha > \alpha_c$ behaves as a function of $\bar{\mu}$ and m [see Eqs. (B54) and (B61) and Fig. 17].

1. Coupled EOMs for relaxation functions

The EOMs derived henceforth are *linearized* with respect to the relaxation functions (unknown quantities). Namely, the mode-mode interactions among various bosonic degrees of freedom (density, current and so on) will be represented by the "mean field" induced by the corresponding relaxation functions. This mean field for the relaxation function is analogous to the self-energy for a one-point Green's function so that it is often dubbed as the relaxation kernel.[35] Being linearized, such EOMs can be easily solved, only to let us express relaxation functions in terms of the relaxation kernel.

These linearized EOMs also have to be *closed* with respect to a set of unknown relaxation functions. Consider, for example, the EOM of the density relaxation function, which is nothing but the continuity equation. This equation contains the current relaxation function. Accordingly, to make coupled EOMs to be closed, we further need the EOM for this current relaxation function, i.e., constitutive equation. The constitutive equation usually involves interactions between the current and other degrees of freedom (DOFs) such as the spin density, sublattice density, and so forth. As such, we further need to derive the EOMs of the relaxation functions associated with these internal DOFs. In this way, we need to make our entire coupled EOMs to be *closed* with respect to a set of unknown relaxation functions.

Let us begin with the continuity equation. Apply the following differential operator from the left-hand side of the Bethe-Salpeter equation Eq. (B1):

$$\delta_0\hat{G}^{-1}(k;q,\omega) \equiv \hat{G}^{R,-1}(k_+,\mu_+) - \hat{G}^{A,-1}(k_-,\mu_-) = \omega\hat{1} - q_\lambda\hat{\gamma}_\lambda - \hat{\Sigma}^R(\mu_+) + \hat{\Sigma}^A(\mu_-).$$

Taking the summation over repeated band indices, we then have

$$[\omega\hat{1} - q_\mu\hat{\gamma}_\mu - \hat{\Sigma}^R + \hat{\Sigma}^A]_{\beta\alpha}\Phi_{\alpha\gamma,\gamma\beta}(k,k';q,\omega) = -[\hat{G}^R(k_+,\mu_+) - \hat{G}^A(k_-,\mu_-)]_{\beta_1\alpha_1}\left\{-\frac{1}{2\pi i}\delta_{\alpha_1\beta_1}\delta_{k,k'} + \sum_{k_1} U^{\rm 2PIR}_{\alpha_1\delta_1,\gamma_1\beta_1}(k,k_1;q,\omega)\Phi_{\delta_1\gamma,\gamma\gamma_1}(k_1,k';q,\omega)\right\}. \quad \text{(B10)}$$

Under the integrals over k and k', the vertex function and the self-energy in Eq. (B10) set off each other,

$$\omega\phi_0(q,\omega) - q\phi_j(q,\omega) = \frac{1}{2\pi i}\sum_{k',\gamma}\{\hat{G}^R_{\gamma\gamma}(k'_+,\mu_+) - \hat{G}^A_{\gamma\gamma}(k'_-,\mu_-)\}. \quad \text{(B11)}$$

Namely, we used the following Ward identity:

$$[\Sigma^R(k_+,\mu_+) - \Sigma^A(k_-,\mu_-)]_{\beta\alpha} \equiv \sum_{k'}\delta\hat{G}_{\beta'\alpha'}(k';q,\omega)U^{\rm 2PIR}_{\alpha'\alpha,\beta\beta'}(k',k;q,\omega),$$

with $\delta\hat{G}(k;q,\omega) \equiv \hat{G}^R(k_+,\mu_+) - \hat{G}^A(k_-,\mu_-)$.

Recall that we are interested in the relaxation functions for sufficiently low-energy and long-wavelength region, only to derive their diffusion pole structure. Thus, regarding ω and q as sufficiently small quantities, we can replace the right-hand side of Eq. (B11) by the spectral function,

$$\omega\phi_0(q,\omega) - q\phi_j(q,\omega) = A_0 + \mathcal{O}(q,\omega), \quad \text{(B12)}$$

where $|A_0|$ stands for the density of state at $\epsilon = \mu$,

$$A_0 \equiv \frac{1}{2\pi i}\sum_k \mathrm{Tr}[\delta\hat{G}(k;0,0)] \simeq -16F_0''\Lambda. \quad \text{(B13)}$$

Equation (B12) is nothing but the continuity equation.

The continuity equation derived above contains the current relaxation function. Thus, we need to next derive an equation of motion for this. The derivation goes along in a quite analogous way as that of the continuity equation. Specifically, to end up with an equation having $\omega\phi_j(q,\omega)$, we will apply the following onto the Bethe-Salpeter equation, instead of $\delta_0\hat{G}^{-1}$,

$$\delta_j\hat{G}^{-1}(k;q,\omega) \equiv \frac{1}{2}[\delta_0\hat{G}^{-1}(k;q,\omega),\hat{q}_\mu\hat{\gamma}_\mu]_+.$$

Since ω and q are sufficiently small, we will keep only its leading-order contributions,

$$\delta_j\hat{G}^{-1}(k;q,\omega) \simeq \left(\omega\frac{\partial F_0'}{\partial\mu} + 2iF_0''\right)\hat{q}_\mu\hat{\gamma}_\mu - q\hat{1}. \quad \text{(B14)}$$

Apply this onto Eq. (B1) and take the sum over k, k', and the band indices. By way of this, we obtain the following constitutive equation:

$$\left(\omega\frac{\partial F_0'}{\partial\mu} + 2iF_0''\right)\phi_j(q,\omega) - q\phi_0(q,\omega)$$
$$= A_j - \sum_{k,k_1}[\hat{\gamma}_j^{\mathrm{L}}(k;q,\omega)]_{\beta_1\alpha_1}$$
$$\times U^{\mathrm{2PIR}}_{\alpha_1\delta_1,\gamma_1\beta_1}(k,k_1;q,\omega)\sum_{k'}\Phi_{\delta_1\gamma,\gamma\gamma_1}(k_1,k';q,\omega). \quad \text{(B15)}$$

A_j and $\hat{\gamma}_j^{\mathrm{L}}(k;q,\omega)$ are defined as follows:

$$A_j \equiv \frac{1}{2\pi i}\sum_k \mathrm{Tr}[\hat{\gamma}_j^{\mathrm{L}}(k;q,\omega)], \quad \text{(B16)}$$

$$\hat{\gamma}_j^{\mathrm{L}}(k;q,\omega)$$
$$\equiv \frac{1}{2}\{\delta\hat{G}(k;q,\omega)\cdot\hat{G}^{R,-1}(k_+,\mu_+)\cdot\hat{q}_\mu\hat{\gamma}_\mu\cdot\hat{G}^R(k_+,\mu_+)$$
$$+\hat{G}^A(k_-,\mu_-)\cdot\hat{q}_\mu\hat{\gamma}_\mu\cdot\hat{G}^{A,-1}(k_-,\mu_-)\cdot\delta\hat{G}(k;q,\omega)\}. \quad \text{(B17)}$$

Contrary to the continuity equation, this equation of motion contains the convolution between the 2PIR vertex function and the response function explicitly. This convolution part describes the interactions between the current relaxation function and the other types of relaxation functions. We will linearize this convolution part with respect to relaxation functions in the following three paragraphs.

To do this, note first the completeness of the γ matrices,

$$\delta_{\gamma\gamma'}\delta_{\delta\delta'} \equiv \frac{1}{4}\sum_{\mu=\{0,1,\cdot,5,15,\cdots,42\}}[\hat{\gamma}_\mu]_{\gamma\delta}[\hat{\gamma}_\mu]_{\delta'\gamma'} \quad \text{(B18)}$$

and that of the spherical harmonic function $Y_{lm}(\hat{\Omega})$,

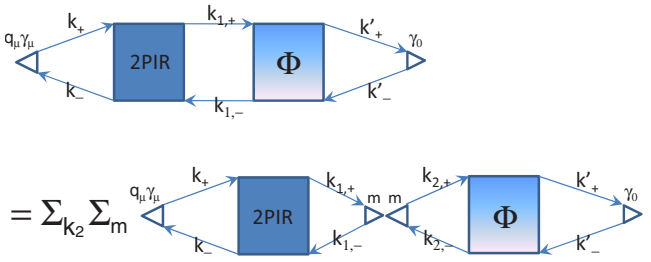

FIG. 16. (Color online) The convolution between the 2PIR vertex function and the response function is replaced by the direct product between the relaxation kernels and relaxation functions, where we used the complete set for a function of k_1, i.e., $f(k_1) \equiv \Sigma_{k_2}\delta(k_1-k_2)f(k_2) \equiv \Sigma_{k_2}\Sigma_m u_m(k_1)\times u_m^*(k_2)f(k_2)$. Namely, u_m constitutes the bare vertex part described by "▷" mark in the figure, while u_m^* constitutes that described by "◁" mark.

$$f(x\hat{\Omega}) \equiv \sum_{l=0}^{\infty}\sum_{m=-l}^{l} Y_{lm}(\hat{\Omega})\sum_{\hat{\Omega}'} Y_{lm}^*(\hat{\Omega}')f(x\hat{\Omega}'), \quad \text{(B19)}$$

where $\hat{\Omega}$ denotes the normalized vector and $\Sigma_{\hat{\Omega}}\cdots$ stands for the two-dimensional integral over the angle direction: $\Sigma_{\hat{\Omega}} \equiv 4\pi$. Using these two completeness relations, we can decouple the convolution part in Eq. (B15) into the sum over the countable numbers of modes (see also Fig. 16),

$$\left(\omega\frac{\partial F_0'}{\partial\mu} + 2iF_0''\right)\phi_j(q,\omega) - q\phi_0(q,\omega)$$
$$= A_j - \frac{1}{4}\sum_{k,k_1}[\hat{\gamma}_j^L(k;q,\omega)]_{\beta_1\alpha_1}U^{\mathrm{2PIR}}_{\alpha_1\delta_1,\gamma_1\beta_1}(k,k_1;q,\omega)$$
$$\times\sum_{\mu=0}^{15}\sum_{l=0}^{\infty}\sum_{m=-l}^{l} Y_{lm}(\hat{k}_1)[\hat{\gamma}_\mu]_{\delta_1\gamma_1}\bar{\phi}_{lm,\mu}(|k_1|;q,\omega). \quad \text{(B20)}$$

Namely, the k_1 dependence of the response function is decomposed into the dependence on its radial coordinate $|k_1|$ and that on the angle coordinate $\hat{k}_1$. At a price for this, the right-hand side contains the summation over the azimuthal and magnetic quantum numbers, l and m. For each l, m, and μ, $\bar{\phi}_{lm,\mu}(x;q,\omega)$ is defined as follows:

$$\bar{\phi}_{lm,\mu}(x;q,\omega) \equiv \sum_{\hat{k}}\sum_{k'}\sum_{\alpha,\beta,\gamma}[\hat{\gamma}_\mu]_{\beta\alpha}Y_{lm}^*(\hat{k})\Phi_{\alpha\gamma,\gamma\beta}(x\hat{k},k';q,\omega). \quad \text{(B21)}$$

Observing this definition, notice that the x dependence of $\bar{\phi}_{lm,\mu}(x;q,\omega)$ and its ω,q dependence can be further *factorized* for *small* ω and q,

$$\bar{\phi}_{lm,\mu}(x;q,\omega) = g_{lm,\mu}(x)\phi_{lm,\mu}(q,\omega). \quad \text{(B22)}$$

This is because, for such small ω and q, the response function appearing in Eq. (B21) is dominated by the diffuson, which depends only on ω and q,

TABLE III. Symmetry of eight modes in the s-wave sector and their symmetries under the spatial inversion $\mathcal{I}$ and the time reversal $\mathcal{T}$. Since $\hat{\gamma}_0$, $\hat{\gamma}_4$, $\hat{\gamma}_5$, and $\hat{\gamma}_{45}$ behave as a scalar quantity under the rotation defined in Eq. (23), we regard them as the "density" associated with the sublattice and spin degrees of freedom. Corresponding to these four types of density, we have four types of "current," which in turn behave as a vector quantity under the rotation.

Label	Density	$\mathcal{T}$	$\mathcal{I}$	label	"Current"	$\mathcal{T}$	$\mathcal{I}$
"0"	$\hat{\gamma}_0$	+	+	"j"	$\hat{q}_\mu \hat{\gamma}_\mu$	−	−
"5"	$\hat{\gamma}_5$	+	+	"5j"	$\hat{q}_\mu \hat{\gamma}_{\mu 5}$	+	−
"4"	$\hat{\gamma}_4$	−	−	"4j"	$\hat{q}_\mu \hat{\gamma}_{\mu 4}$	−	+
"45"	$\hat{\gamma}_{45}$	+	−	"45j"	$\hat{q}_\mu \frac{1}{2}\epsilon_{\mu\nu\rho}\hat{\gamma}_{\nu\rho}$	−	+

$$\Phi_{\alpha\delta,\gamma\beta}(k,k';q,\omega) \simeq -\frac{\alpha}{2\pi i}\hat{G}^R_{\alpha\alpha_1}(k_+,\mu_+)\hat{G}^A_{\beta_1\beta}(k_-,\mu_-) \times [\hat{\Gamma}^d(q,\omega)]_{\alpha_1\delta_1,\gamma_1\beta_1}\hat{G}^R_{\delta_1\delta}(k'_+,\mu_+) \times \hat{G}^A_{\gamma\gamma_1}(k'_-,\mu_-). \tag{B23}$$

By taking the integrals over $\hat{k}$ and k' in Eq. (B21) and keeping only the leading order in small ω and q, one can actually verify this factorization for any l, m, and μ (consult also Appendix D for several examples.)

Without loss of generality, we can assume that $g_{lm,\mu}(x)$ thus obtained is normalized with respect to the integral over the radial direction,

$$\int_0^\Lambda x^2 dx g_{lm,\mu}(x) \equiv 1.$$

Then, corresponding $\phi_{lm,\mu}(q,\omega)$ given in Eq. (B22) becomes the nonzero azimuthal number ($l \neq 0$) generalizations of the relaxation functions defined in Eqs. (B3) and (B4),

$$\phi_{lm,\mu}(q,\omega) \equiv \sum_{k,k'}\sum_{\alpha,\beta,\gamma}[\hat{\gamma}_\mu]_{\beta\alpha}Y^*_{lm}(\hat{k})\Phi_{\alpha\gamma,\gamma\beta}(k,k';q,\omega). \tag{B24}$$

Thus, substitute Eq. (B22) back into Eq. (B20). Then, we finally obtain the constitutive equation, which is fully linearized with respect to these relaxation functions,

$$\left(\omega\frac{\partial F'_0}{\partial\mu} + 2iF''_0\right)\phi_j(q,\omega) - q\phi_0(q,\omega) = A_j - \frac{1}{4}\sum_{l=0}^{\infty}\sum_{m=-l}^{l}\sum_{\mu=0}^{15} \times \left\{\sum_{k,k'}[\hat{\gamma}^L_j(k;q,\omega)]_{\beta\alpha}U^{\mathrm{2PIR}}_{\alpha\delta,\gamma\beta}(k,k';q,\omega) \times [\hat{\gamma}_\mu]_{\delta\gamma}g_{lm,\mu}(|k'|)Y_{lm}(\hat{k}')\right\}\phi_{lm,\mu}(q,\omega). \tag{B25}$$

The second member of its right-hand side described the mean field induced by other relaxation functions, into which the 2PIR vertex function is encoded. This situation is quite analogous to how the one-particle irreducible function (i.e., self-energy) describes the interaction among one-point Green's functions.

Due to this interaction, however, the constitutive equation above also contains relaxation functions $\phi_{lm,\mu}(q,\omega)$ assigned to the higher order harmonic ($l \geq 1$) sector. Thus, to make the final coupled EOMs to be closed, we must also derive the EOM for all of these functions. This is, however, limitless. To make it tractable, we thus need to truncate interactions among these too many modes. In this paper, we will consider the interactions only within the "s-wave" sector. Namely, we will restrict the summation over l, m, and μ in Eq. (B25) to the $l=0$ sector,

$$\phi_{00,\eta}(q,\omega) \equiv \sum_{k,k'}\sum_{\alpha,\beta,\gamma}[\hat{\gamma}_\eta]_{\beta\alpha}\Phi_{\alpha\gamma,\gamma\beta}(k,k';q,\omega).$$

These 16 modes in the s-wave sector further reduce into the eight modes (Table III) when the rotational symmetry is taken into account. Namely, by noting that the response function is invariant under the simultaneous rotation in the pseudospin space and in the momentum space,

$$[\hat{U}_{n,\phi}]_{\alpha'\alpha}[\hat{U}_{n,\phi}]_{\gamma'\gamma}\Phi_{\alpha\delta,\gamma\beta}(k,k;q,\omega)[\hat{U}^\dagger_{n,\phi}]_{\delta\delta'}[\hat{U}^\dagger_{n,\phi}]_{\beta\beta'} \equiv \Phi_{\alpha'\delta',\gamma'\beta'}(R_{n,\phi}k,R_{n,\phi}k';R_{n,\phi}q,\omega),$$

$$\hat{U}_{n,\phi} \equiv e^{(\phi/4)\epsilon_{\mu\nu\rho}n_\mu\hat{\gamma}_\nu\hat{\gamma}_\rho}, \tag{B26}$$

we can derive the following identity:

$$\sum_{\mu=0}^{15}[\hat{\gamma}_\mu]_{\alpha\beta}\phi_{00,\mu}(q,\omega) \equiv \frac{1}{\sqrt{4\pi}}\sum_{a=0}^{45j}[\hat{v}_a(q)]_{\alpha\beta}\phi_a(q,\omega), \tag{B27}$$

with

$$\phi_a(q,\omega) \equiv \sum_{k,k'}\sum_{\alpha,\beta,\gamma}[\hat{v}_a(q)]_{\beta\alpha}\Phi_{\alpha\gamma,\gamma\beta}(k,k';q,\omega),$$

$$(\hat{v}_0,\hat{v}_5,\hat{v}_4,\hat{v}_{45}) \equiv (\hat{\gamma}_0,\hat{\gamma}_5,\hat{\gamma}_4,\hat{\gamma}_{45}),$$

$$(\hat{v}_j,\hat{v}_{5j},\hat{v}_{4j},\hat{v}_{45j}) \equiv \left(\hat{q}_\mu\hat{\gamma}_\mu,\hat{q}_\mu\hat{\gamma}_{5\mu},\hat{q}_\mu\hat{\gamma}_{4\mu},\frac{1}{2}\hat{q}_\mu\epsilon_{\mu\nu\lambda}\hat{\gamma}_{\nu\lambda}\right). \tag{B28}$$

By use of this equality, Eq. (B25) turns out to consist only of those eight functions defined in Eq. (B28),

$$\omega\frac{\partial F_0'}{\partial \mu}\phi_j - q\phi_0 + \sum_{a=0,5,\cdots,45j} \mathcal{M}_{j,a}(q,\omega)\phi_a = A_j, \quad \text{(B29)}$$

$$\mathcal{M}_{a,b}(q,\omega) \equiv 2iF_0''\delta_{ab} + \frac{1}{2^4\pi}\sum_{k,k'} [\hat{\gamma}_a^{\mathrm{L}}(k;q,\omega)]_{\beta\alpha} \times U^{\mathrm{2PIR}}_{\alpha\delta,\gamma\beta}(k,k';q,\omega)[\hat{\gamma}_b^{\mathrm{R}}(k';q,\omega)]_{\delta\gamma}. \quad \text{(B30)}$$

$\hat{\gamma}_a^{\mathrm{L,R}}(k;q,\omega)$ above are given as follows:

$$\hat{\gamma}_a^{\mathrm{L}}(k;q,\omega) \equiv \frac{1}{2}\{\delta\hat{G}(k;q,\omega)\cdot\hat{G}^{R,-1}(k_+,\mu_+)\cdot\hat{v}_a(q)\cdot\hat{G}^{R}(k_+,\mu_+) + \hat{G}^{A}(k_-,\mu_-)\cdot\hat{v}_a(q)\cdot\hat{G}^{A,-1}(k_-,\mu_-)\cdot\delta\hat{G}(k;q,\omega)\}, \quad \text{(B31)}$$

$$\hat{\gamma}_a^{\mathrm{R}}(k;q,\omega) \equiv \hat{v}_a(q)g_{00,a}(|k|). \quad \text{(B32)}$$

$\mathcal{M}_{a,b}(q,\omega)$ defined in Eq. (B30) generally appears in the EOM for the v_a-type relaxation function and plays role of the mean field induced by the v_b-type relaxation functions. Namely, this 8×8 matrix is nothing but the "self-energy" in the matrix-formed EOMs for the s-wave sector [see Eq. (B35)]. Thus, we will refer to $\hat{\mathcal{M}}(q,\omega)$ as the *relaxation kernel* henceforth. Notice that each element of this matrix becomes pure imaginary when its two arguments taken to be zero,

$$\mathcal{M}_{a,b}(q,\omega)^* = -\mathcal{M}_{a,b}(-q,-\omega). \quad \text{(B33)}$$

This can be directly seen from

$$\{\delta\hat{G}(k;q,\omega)\}^* \equiv -\{\delta\hat{G}(k;-q,-\omega)\}^t,$$

$$\{U^{\mathrm{2PIR}}_{\alpha\delta,\gamma\beta}(k,k';q,\omega)\}^* = U^{\mathrm{2PIR}}_{\beta\gamma,\delta\alpha}(k,k';-q,-\omega). \quad \text{(B34)}$$

The EOMs for the other six s-wave modes can be derived in parallel with that for the current relaxation function. Specifically, we will begin with the Bethe-Salpeter equation applied by the following, instead of Eq. (B14):

$$\delta_a\hat{G}^{-1}(k;q,\omega) \equiv \frac{1}{2}[\delta_0\hat{G}^{-1}(k;q,\omega),\hat{v}_a(q)]_+,$$

with $\hat{v}_a(q)$ taken to be $\hat{\gamma}_5,\hat{\gamma}_4,\ldots,\frac{1}{2}\hat{q}_\mu\epsilon_{\mu\nu\rho}\hat{\gamma}_\nu\hat{\gamma}_\rho$, respectively. Going through the same procedure as described so far, we will reach the constitutive equations for these remaining six modes. Combined with Eqs. (B12) and (B29), such equations consist of the following 8×8 matrix-formed EOMs,

$$[\hat{\mathcal{K}}(q,\omega)+\hat{\mathcal{M}}(q,\omega)]\cdot\hat{\phi}(q,\omega) \equiv \hat{A}(q,\omega). \quad \text{(B35)}$$

$\hat{\phi}(q,\omega)$ and $\hat{A}(q,\omega)$ read,

$$\hat{\phi}^t \equiv [\phi_0,\phi_j,\phi_5,\phi_{5j},\phi_4,\phi_{4j},\phi_{45},\phi_{45j}],$$

$$\hat{A}^t \equiv [A_0,A_j,A_5,A_{5j},A_4,A_{4j},A_{45},A_{45j}],$$

latter of which is defined as follows:

$$A_a(q,\omega) \equiv \frac{1}{2\pi i}\sum_k \mathrm{Tr}[\hat{\gamma}_a^{\mathrm{L}}(k;q,\omega)]. \quad \text{(B36)}$$

$\hat{\mathcal{K}}(q,\omega)$ and $\hat{\mathcal{M}}(q,\omega)$ are defined as follows:

$$\hat{\mathcal{K}} \equiv \begin{bmatrix} \hat{\mathcal{K}}_1 & \hat{0} \\ \hat{0} & \hat{\mathcal{K}}_2 \end{bmatrix}, \quad \hat{\mathcal{M}} \equiv \begin{bmatrix} \hat{\mathcal{M}}_1 & \hat{0} \\ \hat{0} & \hat{\mathcal{M}}_2 \end{bmatrix},$$

$$\hat{\mathcal{K}}_1 \equiv \begin{bmatrix} \omega & -q & & \\ -q & \omega c^{-1} & & \\ \omega d^{-1}+2ie^{-1} & & \omega c^{-1} & \\ & & & \omega c^{-1} \end{bmatrix},$$

$$\hat{\mathcal{K}}_2 \equiv \begin{bmatrix} \omega c^{-1} & & & \\ & \omega c^{-1} & & \omega d^{-1}+2ie^{-1} \\ & & \omega c^{-1} & -q \\ & \omega d^{-1}+2ie^{-1} & -q & \omega c^{-1} \end{bmatrix}, \quad \text{(B37)}$$

$$\hat{\mathcal{M}}_1 \equiv \begin{bmatrix} 0 & & 0 & \\ & \mathcal{M}_{j,j} & & \mathcal{M}_{j,5j} \\ \mathcal{M}_{5,0} & & \mathcal{M}_{5,5} & \\ & \mathcal{M}_{5j,j} & & \mathcal{M}_{5j,5j} \end{bmatrix},$$

$$\hat{\mathcal{M}}_2 \equiv \begin{bmatrix} \mathcal{M}_{4,4} & & \mathcal{M}_{4,45} & \\ & \mathcal{M}_{4j,4j} & & \mathcal{M}_{4j,45j} \\ \mathcal{M}_{45,4} & & \mathcal{M}_{45,45} & \\ & \mathcal{M}_{45j,4j} & & \mathcal{M}_{45j,45j} \end{bmatrix}, \quad \text{(B38)}$$

with

$$c^{-1} \equiv \frac{\partial F_0'}{\partial\mu}, \quad d^{-1} \equiv \frac{\partial F_5'}{\partial\mu}, \quad e^{-1} \equiv F_5''. \quad \text{(B39)}$$

By solving Eq. (B35), one can obtain the asymptotic expressions for the relaxation functions for small ω and q,

$$\phi_0(q,\omega) \simeq \frac{A_0}{\omega+iDq^2}, \quad \phi_5(q,\omega) \simeq \frac{A_0B_0}{\omega+iDq^2}, \ldots, \quad \text{(B40)}$$

where $|A_0|$ stands for the density of state [see Eq. (B13)]. The (renormalized) diffusion constant D used above and other coupling constants are expressed only in terms of the relaxation kernels estimated at $\omega,q=0$,

$$D \equiv i\left\{\frac{\mathcal{M}_{5j,5j}}{\mathcal{M}_{jj}\mathcal{M}_{5j,5j}-\mathcal{M}_{5j,j}\mathcal{M}_{j,5j}}\right\}_{|q,\omega=0}, \quad \text{(B41)}$$

$$B_0 \equiv -\left\{\frac{2iF_5''+\mathcal{M}_{5,0}}{\mathcal{M}_{5,5}}\right\}_{q,\omega=0}. \quad \text{(B42)}$$

Equations (B41) and (B30) become the essential building blocks of our gap equation (see below).

2. Gap equation and its solution

As was shown in Sec. IV, the charge diffusion mode and parity diffusion mode equally dominates the diffuson in the massless case ($Dl^{-2} \geq \tau_{\text{topo}}^{-1}$), while the parity mode becomes ineffective in the presence of the relatively large topological mass ($Dl^{-2} \leq \tau_{\text{topo}}^{-1}$) [see Eqs. (106), (98), and (102)]. Corresponding to these two limiting cases, we will derive two types of gap equations and their solutions in this section.

a. For m=0 case

Let us begin with the zero topological mass case first. In this case, we will sum up Eqs. (107) and (108) since $f_3 \equiv f_4$. With use of Eq. (96) and $a_{2,3,4} \equiv 0$, such a summand takes on a following form:

$$\hat{\Gamma}^d(q,\omega)_{|F_5 \equiv 0} = -\frac{a_0 f_4}{4}(\hat{1} + \hat{T}_1 + \hat{S}_1 + \hat{S}_2). \tag{B43}$$

In Sec. IV B, we have observed that the overall factor, $a_0 f_4$, has the diffusion pole as in Eq. (98), where its *bare* expression was calculated explicitly. Namely, by keeping track of the small q effect in Eq. (78), we obtained the bare diffusion constant as in Eq. (99). Instead of such bare expressions, however, we will describe henceforth this $a_0 f_4$ in terms of the *renormalized* diffusion constant defined by Eq. (B41). Namely, we want $a_0 f_4$ to be given by the relaxation kernels, only to obtain the *self-consistent* equation for the diffusion constant.

To do this, notice that relaxation functions for *small* q and ω are dominated by the diffuson as in Eq. (B23). Thus, by substituting Eq. (B43) into Eqs. (B23) and (B3), we will first express the density relaxation function in terms of $a_0 f_4$,

$$\phi_0(q,\omega) \simeq -64\pi i \alpha \Lambda^2 a_0 f_4. \tag{B44}$$

The factor Λ^2 in the right-hand side stems from the momentum integral over k and k' in Eq. (B3); Λ is the ultraviolet cutoff of the momentum integral. Then, we will equate this with $\phi_0(q,\omega)$ obtained in step (i), i.e., Eq. (B40). By doing this, $a_0 f_4$ is expressed in terms of relaxation kernels,

$$-64\pi i \alpha a_0 f_4 \equiv \frac{1}{\Lambda^2}\frac{A_0}{\omega + iDq^2}. \tag{B45}$$

Namely, the diffusion constant D in the right-hand side was already given by the relaxation kernels as in Eq. (B41).

Substituting this back into Eq. (B43), we obtain the Cooperon at small ω and $k+k'$,

$$\begin{aligned}\hat{U}^{\text{coop}}(k+k',\omega) &= -\frac{\alpha a_0 f_4}{4}(\hat{1} - \hat{T}_1 - \hat{S}_1 + \hat{S}_2) \\ &= \frac{1}{2^8 \pi i}\frac{1}{\Lambda^2}\frac{A_0}{\omega + iD(k+k')^2}(\hat{1} - \hat{T}_1 - \hat{S}_1 + \hat{S}_2),\end{aligned} \tag{B46}$$

The diffusion constant D in Eq. (B46) is now given by the relaxation kernels, via Eq. (B41). These relaxation kernels are in turn defined by the 2PIR vertex function, via Eq. (B30). The 2PIR vertex function is usually dominated by the Cooperon given by Eq. (B46), at around $k+k' \simeq 0$. As such, we will replace (approximate) the 2PIR vertex function in Eq. (B30) by this asymptotic form of the Cooperon, i.e., Eq. (B46). By way of this, we obtain closed coupled equations for the (renormalized) diffusion constant D,

$$D \equiv i\frac{\mathcal{M}_{5j,5j}}{\mathcal{M}_{jj}\mathcal{M}_{5j,5j} - \mathcal{M}_{5j,j}\mathcal{M}_{j,5j}}, \tag{B47}$$

$$\begin{aligned}\mathcal{M}_{a,b} \equiv 2iF_0''\delta_{a,b} + \frac{|A_0|}{2^{12}\pi^2 D\Lambda^2}\int\int_{L^{-1}<|k+k'|<l^{-1}} d^3k d^3k' \\ \times \frac{\{\hat{\gamma}_a^{\text{L}}(k)\}_{\beta\alpha}\{\hat{1} - \hat{T}_1 - \hat{S}_1 + \hat{S}_2\}_{\alpha\delta,\gamma\beta}\{\hat{\gamma}_b^{\text{R}}(k')\}_{\delta\gamma}}{|k+k'|^2}.\end{aligned} \tag{B48}$$

Since Eq. (B46) is valid only for small $|k+k'|$, we have imposed the additional constraint $|k+k'| < l^{-1}$ into these integral variables. One might regard this upper limit as the mean-free path. We have already taken in Eq. (B48) both ω and q to be zero. Thus, $\hat{\gamma}^{\text{L,R}}(k)$ in the right-hand side stands for $\hat{\gamma}^{\text{L,R}}(k;q,\omega)$ estimated there;

$$\hat{\gamma}_a^{\text{L}}(k) \equiv \hat{\gamma}_a^{\text{L}}(k;0,0),$$

$$\hat{\gamma}_a^{\text{R}}(k) \equiv \hat{v}_a \times g_{00,a}(|k|),$$

where $\hat{v}_a$ was already defined in Eq. (B28). The normalized real-valued function $g_{00,a}(x)$ used above is given only in terms of F_0. For example, $g_{00,j}(x)$ is given as follows:

$$g_{00,j}(x) \equiv \frac{4}{\pi}\frac{1}{\mathcal{N}_j}\frac{1}{|F_0^2 - x^2|^2}\left\{1 + \frac{8}{3}\frac{x^2 F_0'^2}{|F_0^2 - x^2|^2}\right\}, \tag{B49}$$

with its normalization factor N_j,

$$\mathcal{N}_j = \frac{1}{F_0''}\left\{1 + \frac{1}{3}\left(\frac{F_0'}{F_0''}\right)^2\right\} \tag{B50}$$

(see Appendix D for its derivation). Thus, Eqs. (B47) and (B48) constitute closed coupled equations for the diffusion constant.

To solve this gap equation, notice first that the coupling between the current and the $\hat{\gamma}_5$-type current is disconnected in the massless case; $\mathcal{M}_{j,5j} = 0$. This can be seen directly from

$$(\hat{1} - \hat{T}_1 - \hat{S}_1 + \hat{S}_2)_{\alpha\delta,\gamma\beta}\hat{q}_\mu[\hat{\gamma}_{\mu 5}]_{\delta\gamma} = 0, \tag{B51}$$

which leads to $D \equiv i/\mathcal{M}_{j,j}$. As a result of this, Eqs. (B47) and (B48) become linear in D,

$$\begin{aligned}\frac{1}{D} = 2F_0'' - \frac{A_0 F_0''}{2^7\pi^2 D}\frac{1}{\Lambda^2}\int\int_{L^{-1}<|k+k'|<l^{-1}} d^3k d^3k' \\ \times \frac{g_{00,j}(|k'|)}{|k+k'|^2}\frac{[-(F_0')^2 - (F_0'')^2 + k^2] - 2(k\cdot\hat{q})^2}{[(F_0')^2 - (F_0'')^2 - k^2]^2 + 4(F_0')^2(F_0'')^2}.\end{aligned} \tag{B52}$$

Using Eqs. (B49) and (B50), we can readily evaluate the momentum integral in the right-hand side of Eq. (B52). To do this, we introduce a new integral variable $q' \equiv k+k'$ so

that $dkdk' \equiv dkdq'$. Moreover, we approximate $g_{00,j}(|k-q'|)$ in the integrand by $g_{00,j}(|k|)$ since $g_{00,j}(x)$ is a slowly varying function in the scale of l^{-1}. These treatments give us the following expression for $2D\tau^{-1}$:

$$2D\tau^{-1} \equiv 1 + \frac{1}{6}\frac{l^{-1}-L^{-1}}{\Lambda}\frac{\tau^{-2}+\frac{1}{2}\bar{\mu}^2}{\tau^{-2}+\frac{1}{3}\bar{\mu}^2}, \tag{B53}$$

where we used $A_0 \equiv -16F_0''\Lambda$ and $F_0 \equiv \bar{\mu} + i\tau^{-1}$. Observing this expression, notice that the second member of the right-hand side is nothing but the quantum correction to the diffusion constant, which basically corresponds to the AWL correction to the conductivity.

b. For $m \neq 0$ case

In the presence of relatively large topological mass, i.e., $Dl^{-2} \leq \tau_{\text{topo}}^{-1}$, the parity diffusion mode becomes the high-energy degree of freedom. As such, only the charge diffusion mode in Eq. (106) contributes the diffuson. With Eq. (95), such diffuson is given as follows:

$$\hat{\Gamma}^d(q,\omega)_{|F_5\neq 0} = -\frac{sf_4}{8}\left\{\frac{1+t^2}{2}(\hat{1}+\hat{T}_4)(\hat{1}+\hat{S}_1) + \frac{1-t^2}{2}(\hat{1}+\hat{T}_4) \times(\hat{T}_1+\hat{S}_2) + t(\hat{T}_2+\hat{T}_3)(\hat{1}+\hat{S}_1)\right\}, \tag{B54}$$

where s and t are defined by a_{04}, a_1, and a_{23},

$$a_{04} \equiv s\frac{1+t^2}{2}, \quad -3a_1 \equiv s\frac{1-t^2}{2}, \quad -a_{23} \equiv st.$$

Contrary to the previous subsection, the tensor part of the diffuson depends on the model parameters through the factor t. As such, we will employ in this case not only the diffusion constant D but also this tensor-form factor t as the "mean-field parameters," which should be self-consistently determined. In other words, both of them should be given by the relaxation kernels, as in Eq. (B41).

To do this, we will first calculate both the density relaxation function ϕ_0 and the sublattice density relaxation function ϕ_5 by the use of Eq. (B54). Namely, we will substitute Eq. (B54) into Eqs. (B23) and (B28), only to obtain these two functions in terms of sf_4 and t first. The relaxation functions thus calculated read as follows:

$$\phi_0(q,\omega) \simeq -32\pi\alpha\Lambda^2 isf_4, \tag{B55}$$

$$\phi_5(q,\omega) \simeq 32\pi\alpha\Lambda^2 istf_4. \tag{B56}$$

Then, we will equate Eqs. (B55) and (B56) with the first two members of Eq. (B40), respectively. By way of this, f_4 and t can be given in terms of the relaxation kernels,

$$sf_4 \equiv \frac{1}{32\pi\alpha}\frac{1}{\Lambda^2}\frac{|A_0|}{i\omega - Dq^2}, \tag{B57}$$

$$t \equiv -B_0 \equiv \left\{\frac{2iF_5'' + \mathcal{M}_{5,0}}{\mathcal{M}_{5,5}}\right\}_{|q,\omega=0}. \tag{B58}$$

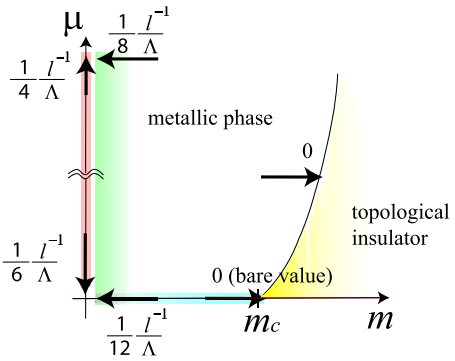

FIG. 17. (Color online) A summary of several limiting values of the quantum correction of the diffusion constant. Equation (B60) corresponds to the green shaded region.

By substituting these two back into Eq. (B54), we can express the diffuson only in terms of the relaxation kernels. When its hole line time reversed, the corresponding Cooperon is readily derived,

$$U^{\text{coop}}(k+k',\omega) \simeq \frac{1}{2^9\pi i}\frac{1}{\Lambda^2}\frac{A_0}{\omega + iD(k+k')^2} \times\{(1+t^2)(\hat{1}+\hat{T}_4)(\hat{1}-\hat{S}_1) - (1-t^2)(\hat{1}-\hat{T}_4)(\hat{T}_1-\hat{S}_2) + 2t(\hat{T}_2+\hat{T}_3)(\hat{1}-\hat{S}_1)\}. \tag{B59}$$

The tensor-form factor t and the diffusion constant D appearing in the right-hand side above are already given by the relaxation kernels, via Eqs. (B58) and (B41). Such relaxation kernels are given by the 2PIR vertex function [see Eq. (B30)]. Thus, as in the previous subsection, we will approximate the 2PIR vertex function by Eq. (B59). In terms of this substitution, we arrive at a closed coupled equation for the diffusion constant D and the tensor-form factor t, whose explicit expressions are given in Appendix C.

When solving this gap equation, we can see how the quantum correction to the diffusion constant behaves as a function of m and μ. Several limiting values are summarized in Fig. 17. Especially, in the zero-mass limit i.e., $m=0+$, the solution of the gap equation reduces to a following simple function of $F_0 \equiv \bar{\mu} + i\tau^{-1}$:

$$\lim_{\bar{m}\to 0+} 2D\tau^{-1} = 1 + \frac{1}{12}\frac{l^{-1}-L^{-1}}{\Lambda}\frac{\tau^{-2}+\frac{1}{2}\bar{\mu}^2}{\tau^{-2}+\frac{1}{3}\bar{\mu}^2}, \tag{B60}$$

Comparing this with Eq. (B53), one can easily see that the quantum correction to the diffusion constant is actually *half* of that for $m=0$ case.

The discrepancy between Eqs. (B53) and (B60) is responsible for the Cooperon term associated with the parity diffusion mode. To see this explicitly, note first that a_2, a_3, and a_4 reduce to zero in the limit of $m \to 0+$. Then, Eqs. (113) and (114) in this limit read as follows:

$$\lim_{m\to 0+} \hat{U}_1^c = -\{(\hat{1}-\hat{T}_1-\hat{S}_1+\hat{S}_2)+\hat{T}_4\cdot(\hat{1}+\hat{T}_1-\hat{S}_1-\hat{S}_2)\}, \tag{B61}$$

$$\lim_{m\to 0+} \hat{U}_2^c = -\{(\hat{1}-\hat{T}_1-\hat{S}_1+\hat{S}_2)-\hat{T}_4\cdot(\hat{1}+\hat{T}_1-\hat{S}_1-\hat{S}_2)\}. \tag{B62}$$

Observing these expressions, notice that the second members of both Eq. (B61) and (B62) are totally ineffective in the current-type relaxation kernels,

$$\{\hat{T}_4\cdot(\hat{1}+\hat{T}_1-\hat{S}_1-\hat{S}_2)\}_{\alpha\delta,\gamma\beta}\hat{q}_\mu[\hat{\gamma}_\mu]_{\delta\gamma}=0, \tag{B63}$$

$$\{\hat{T}_4\cdot(\hat{1}+\hat{T}_1-\hat{S}_1-\hat{S}_2)\}_{\alpha\delta,\gamma\beta}\hat{q}_\mu[\hat{\gamma}_{\mu 5}]_{\delta\gamma}=0. \tag{B64}$$

The consequences of these two equations are twofold. The second equation in combination with Eq. (B51) leads $\mathcal{M}_{j,5j}\equiv 0$ first. Thus, we have $D\equiv\frac{i}{\mathcal{M}_{jj}}$ again, which indicates that $\mathcal{M}_{j,j}$ originated from Eq. (B61) and that from Eq. (B62) contribute to the quantum correction in an *additive* way. Equation (B63) moreover indicates that these two quantum corrections have the *same magnitude* and *sign*. In other words, the quantum correction in Eq. (B53) can be divided into two parts,

$$2D_{|\bar{m}=0}\tau^{-1} = 1+\frac{1}{12}\frac{l^{-1}-L^{-1}}{\Lambda}\frac{\tau^{-2}+\frac{1}{2}\bar{\mu}^2}{\tau^{-2}+\frac{1}{3}\bar{\mu}^2} + \frac{1}{12}\frac{l^{-1}-L^{-1}}{\Lambda}\frac{\tau^{-2}+\frac{1}{2}\bar{\mu}^2}{\tau^{-2}+\frac{1}{3}\bar{\mu}^2}.$$

Each of these two quantum corrections is originated from Eq. (B61) and (B62), respectively. Since we have already ignored Eq. (B62) for the $m\neq 0$ case, the resulting solution has only single 1/12, as in Eq. (B60).

APPENDIX C: MEAN-FIELD EQUATION FOR $m\neq 0$ CASE

The mean-field equation for the diffusion constant D and t in the presence of the finite topological mass m is given as follows:

$$D\equiv i\frac{\mathcal{M}_{5j,5j}}{\mathcal{M}_{jj}\mathcal{M}_{5j,5j}-\mathcal{M}_{5j,j}\mathcal{M}_{j,5j}}, \quad t\equiv\frac{2iF_5''+\mathcal{M}_{5,0}}{\mathcal{M}_{5,5}},$$

with the relaxation kernels $\mathcal{M}_{a,b}$ being given by D and t self-consistently,

$$\mathcal{M}_{a,b}\equiv 2iF_0''\delta_{a,b}+\frac{|A_0|}{2^{13}\pi^2 D}\frac{1}{\Lambda^2}\int\int_{0<|k+k'|<l^{-1}} d^3k d^3k'\frac{1}{|k+k'|^2} \times\{\hat{\gamma}_a^{\mathrm{L}}(k)\}_{\beta\alpha}\{(1+t^2)(\hat{1}+\hat{T}_4)(\hat{1}-\hat{S}_1) -(1-t^2)(\hat{1}-\hat{T}_4)(\hat{T}_1-\hat{S}_2) +2t(\hat{T}_2+\hat{T}_3)(\hat{1}-\hat{S}_1)\}_{\alpha\delta,\gamma\beta}\{\hat{\gamma}_a^{\mathrm{R}}(k')\}_{\delta\gamma}.$$

Note that $\hat{\gamma}^{\mathrm{L,R}}(k)$ above are previously defined,

$$\hat{\gamma}_a^{\mathrm{L}}(k)\equiv\frac{1}{2}\{\delta\hat{G}(k;0,0)\cdot\hat{G}^{R,-1}(k,\mu)\cdot\hat{v}_a\cdot\hat{G}^R(k,\mu) +\hat{G}^A(k,\mu)\cdot\hat{v}_a\cdot\hat{G}^{A,-1}(k,\mu)\cdot\delta\hat{G}(k;0,0)\},$$

$$\hat{\gamma}_a^{\mathrm{R}}(k)\equiv\hat{v}_a\times g_{00,a}(|k|),$$

with $\hat{v}_a$ for $a=0,5,j$ and $5j$ given in Eq. (B28). $g_{00,a}(x)$ used in $\hat{\gamma}_a^{\mathrm{R}}(k)$ are given in terms of the one-point Green's functions (F_0 and F_5) and the tensor-form factor t,

$$g_{00,0}(x)\propto\frac{x^2+\{(|F_0|^2+|F_5|^2)-t(F_0^*F_5+F_0F_5^*)\}}{|(a+ib)^2-x^2|^2},$$

$$g_{00,5}(x)\propto\frac{tx^2-\{t(|F_0|^2+|F_5|^2)-(F_0^*F_5+F_0F_5^*)\}}{|(a+ib)^2-x^2|^2},$$

$$g_{00,j}(x)\propto\left\{\frac{F_0''-tF_5''}{|(a+ib)^2-x^2|^2}+\frac{8}{3}\frac{ab(F_0'-tF_5')x^2}{|(a+ib)^2-x^2|^4}\right\},$$

$$g_{00,5j}(x)\propto\left\{\frac{F_5'-tF_0'}{|(a+ib)^2-x^2|^2}-\frac{8}{3}\frac{ab(F_5''-tF_0'')x^2}{|(a+ib)^2-x^2|^4}\right\},$$

with $(a+ib)^2\equiv F_0^2-F_5^2$.

APPENDIX D: DERIVATION OF $g_{00,a}(x)$

Starting from the Bethe-Salpeter (BS) equation for the response function, we have derived in Appendix B 1 the EOMs for the various types of relaxation functions. Such coupled EOMs have two features; they are closed and *linearized* with respect to the relaxation functions. Because of these two features, we can solve them for the relaxation functions. Out of this solution, we can relate the renormalized diffusion constant with the 2PIR (two-particle irreducible) vertex function. This relation in turn becomes an essential building block of the self-consistent loop of the diffusion constant (see Appendix B).

To obtain such linearized EOMs, we need to reduce the convolution part between the 2PIR vertex function and the response function into the simple product between relaxation kernels and relaxation functions. For this purpose, we have introduced the completeness in the space of the integral variable, say y or w, associated with this convolution,

$$\sum_a u_a(y)\cdot u_a^*(w)\equiv\delta(y-w).$$

Namely, by use of this, any convolution in principle can be decomposed into a simple product,

$$\int dy f(\ldots,y)g(y,\ldots) \equiv\sum_a\int dy f(\ldots,y)u_a(y)\cdot\int dw u_a^*(w)g(w,\ldots).$$

In the current context, $f(\ldots,y)$ corresponds to the 2PIR ver-

tex function, while $g(w,\cdots)$ to the response function. Therefore, $\int dy \ldots f(\ldots,y)u_a(y)$ corresponds to the relaxation kernels, while $\int dw u_a^*(w)g(w,\ldots)\ldots$ does to the relaxation functions (see also Appendix B 1). The trade off for this decomposition is therefore the sum over *infinite* (but countable) numbers of modes specified by a.

To be more specific, we did this decomposition systematically, based on the completeness relation of the γ matrices and the spherical harmonic function $Y_{lm}(\hat{\Omega})$,

$$\int dw u_a^*(w)g(w,\ldots) \to \sum_{\hat{k}} \sum_{\alpha,\beta} [\hat{\gamma}_\mu]_{\beta\alpha} Y_{lm}^*(\hat{k}) \Phi_{\alpha\ldots,\ldots\beta}(|k|\hat{k},\ldots). \tag{D1}$$

As such, the momentum integral only over the angle direction, $\hat{k}$, is taken, while that over its radial direction, $|k|$, is *not* taken. As for the convolution with respect to this radial direction, we simply replace the $|x|$ dependence of $\Phi\ldots(|x|\hat{x},\ldots)$ by some real-valued function $g\ldots(|x|)$. Namely, we rewrite the right-hand side of Eq. (D1) as follows:

$$\sum_{\hat{k}} \sum_{\alpha,\beta} [\hat{\gamma}_\mu]_{\beta\alpha} Y_{lm}^*(\hat{k}) \Phi_{\alpha\ldots,\ldots\beta}(|k|\hat{k},\ldots) = g_{lm,\mu}(|k|) \sum_{k} \sum_{\alpha,\beta} [\hat{\gamma}_\mu]_{\beta\alpha} Y_{lm}^*(\hat{k}) \Phi_{\alpha\ldots,\ldots\beta}(k,\ldots). \tag{D2}$$

Let us justify this treatment in the followings. In the response function, $\Phi_{\alpha\delta,\gamma\beta}(k,k';q,\omega)$, q and ω are associated with the external momentum and frequency for the bosonic degrees of freedom. We can take these two to be small, as far as the relaxation functions for the long-wavelength and low-energy region is concerned. Then, such a response function is usually dominated by the diffuson $\hat{\Gamma}^d(q,\omega)$ [see Eq. (B23)]. As a result of this, the $|k|$ dependence in the left-hand side of Eq. (D2) and its q, ω dependence can be factorized at the leading order in small q and ω,

$$\sum_{k'} \sum_{\hat{k}} \sum_{\alpha,\beta,\gamma} [\hat{\gamma}_\mu]_{\beta\alpha} Y_{lm}^*(\hat{k}) \Phi_{\alpha\gamma,\gamma\beta}(x\hat{k},k';q,\omega) = g_{lm,\mu}(x) \sum_{k,k'} \sum_{\alpha,\beta,\gamma} [\hat{\gamma}_\mu]_{\beta\alpha} Y_{lm}^*(\hat{k}) \Phi_{\alpha\gamma,\gamma\beta}(k,k';q,\omega) = g_{lm,\mu}(x) \times \phi_{lm,\mu}(q,\omega). \tag{D3}$$

To see this factorization more explicitly, one can take the following steps: (i) substitute the asymptotic tensor form of the diffuson into Eq. (B23) and the left-hand side of Eq. (D3), (ii) take the integral and the sum over $\hat{k}$, k', α, β, and γ in Eq. (D3), and (iii) retain the leading order in small q and ω. By way of this, one can reach the factorization given in the right-hand side of Eq. (D3) with a specific $g_{lm,\mu}(x)$.

For example, let us follow these prescriptions in the case of zero topological mass case. Observing Eq. (B43), notice first the following relation:

$$\hat{\Gamma}^d_{\alpha\delta,\gamma\beta}(q,\omega)_{|F_5\equiv 0}[\hat{\gamma}_\mu]_{\delta,\gamma} \equiv 0, \tag{D4}$$

for $\mu=1,2,3$. Using this, one can readily check that the diffuson in this case turns out to be proportional to the unit matrix when its right-hand side is traced out,

$$\sum_{\delta,\gamma} \hat{\Gamma}^d_{\alpha\delta,\gamma\beta}(q,\omega)_{|F_5=0} \sum_{k',\epsilon} \hat{G}^R_{\delta\epsilon}(k'_+,\mu_+)\hat{G}^A_{\epsilon\gamma}(k'_-,\mu_-) = \frac{1}{\omega + iDq^2} \sum_{k'} \frac{|F_0|^2 + k'^2}{|F_0^2 - k'^2|^2} \delta_{\alpha\beta}.$$

As such, to obtain the normalized function $g_{00,a}(x)$ in the massless case, we have only to calculate the following quantity up to the leading order in small ω and q:

$$\sum_{\hat{k},k',\delta,\alpha,\beta} [\hat{v}_a(q)]_{\beta\alpha} \Phi_{\alpha\delta,\delta\beta}(k,k';q,\omega) \propto \frac{1}{i\omega - Dq^2} \sum_{\hat{k}} \sum_{\alpha,\delta,\rho} \hat{G}^R_{\delta\alpha}(k_+,\mu_+)\hat{G}^A_{\alpha\rho}(k_-,\mu_-)[\hat{v}_a(q)]_{\rho\delta}.$$

For example, taking the current component as $\hat{v}_a(q)$ above, we have

$$\sum_{\hat{k},k',\alpha,\beta,\delta} [\hat{q}_\mu \hat{\gamma}_\mu]_{\beta\alpha} \Phi_{\alpha\delta,\delta\beta}(k,k';q,\omega) \propto -\frac{q}{i\omega - Dq^2} \left\{ \frac{1}{|F_0^2 - k^2|^2} + \frac{8}{3} \frac{F_0'^2 k^2}{|F_0^2 - k^2|^4} \right\} + \mathcal{O}(q^2,\omega).$$

Observing the right-hand side, one can then convince oneself of Eq. (D3). Moreover, the normalized real-valued function $g_{00,j}(x)$ will be obtained as in Eqs. (B50) and (B51).

[1] S. Murakami, N. Nagaosa, and S.-C. Zhang, Science **301**, 1348 (2003).
[2] J. Sinova, D. Culcer, Q. Niu, N. A. Sinitsyn, T. Jungwirth, and A. H. MacDonald, Phys. Rev. Lett. **92**, 126603 (2004).
[3] Y. K. Kato, R. C. Myers, A. C. Gossard, and D. D. Awschalom, Science **306**, 1910 (2004).
[4] J. Wunderlich, B. Kästner, J. Sinova, and T. Jungwirth, Phys. Rev. Lett. **94**, 047204 (2005).
[5] C. L. Kane and E. J. Mele, Phys. Rev. Lett. **95**, 146802 (2005).
[6] C. L. Kane and E. J. Mele, Phys. Rev. Lett. **95**, 226801 (2005).
[7] B. A. Bernevig and S.-C. Zhang, Phys. Rev. Lett. **96**, 106802 (2006).
[8] Y. Hatsugai, Phys. Rev. Lett. **71**, 3697 (1993).
[9] C. Wu, B. A. Bernevig, and S.-C. Zhang, Phys. Rev. Lett. **96**, 106401 (2006).
[10] C. Xu and J. E. Moore, Phys. Rev. B **73**, 045322 (2006).
[11] L. Fu and C. L. Kane, Phys. Rev. B **74**, 195312 (2006).
[12] T. Fukui and Y. Hatsugai, Phys. Rev. B **75**, 121403(R) (2007).
[13] B. A. Bernevig, T. L. Hughes, and S.-C. Zhang, Science **314**, 1757 (2006).

[14] M. König, S. Wiedmann, C. Brune, A. Roth, H. Buhmann, L. W. Molenkamp, X. L. Qi, and S. C. Zhang, Science **318**, 766 (2007).
[15] L. Fu, C. L. Kane, and E. J. Mele, Phys. Rev. Lett. **98**, 106803 (2007).
[16] R. Roy, arXiv:cond-mat/0607531 (unpublished).
[17] J. E. Moore and L. Balents, Phys. Rev. B **75**, 121306(R) (2007).
[18] S. Murakami, Phys. Rev. Lett. **97**, 236805 (2006).
[19] D. Hsieh, D. Qian, L. Wray, Y. Xia, Y. S. Hor, R. J. Cava, and M. Z. Hasan, Nature (London) **452**, 970 (2008).
[20] A. P. Schnyder, S. Ryu, A. Furusaki, and A. W. W. Ludwig, Phys. Rev. B **78**, 195125 (2008).
[21] E. Abrahams, P. W. Anderson, D. C. Licciardello, and T. V. Ramakrishnan, Phys. Rev. Lett. **42**, 673 (1979).
[22] S. Murakami, New J. Phys. **9**, 356 (2007); New. J. Phys. **10**, 029802(E) (2008).
[23] S. Murakami and S. Kuga, Phys. Rev. B **78**, 165313 (2008).
[24] J. C. Y. Teo, L. Fu, and C. L. Kane, Phys. Rev. B **78**, 045426 (2008).
[25] M. Onoda, Y. Avishai, and N. Nagaosa, Phys. Rev. Lett. **98**, 076802 (2007).
[26] H. Obuse, A. Furusaki, S. Ryu, and C. Mudry, Phys. Rev. B **76**, 075301 (2007).
[27] A. M. Essin and J. E. Moore, Phys. Rev. B **76**, 165307 (2007).
[28] P. M. Ostrovsky, I. V. Gornyi, and A. D. Mirlin, Phys. Rev. Lett. **98**, 256801 (2007).
[29] S. Ryu, C. Mudry, H. Obuse, and A. Furusaki, Phys. Rev. Lett. **99**, 116601 (2007).
[30] K. Nomura, M. Koshino, and S. Ryu, Phys. Rev. Lett. **99**, 146806 (2007).
[31] J. H. Bardarson, J. Tworzydlo, P. W. Brouwer, and C. W. J. Beenakker, Phys. Rev. Lett. **99**, 106801 (2007).
[32] H. Aoki and T. Ando, Phys. Rev. Lett. **54**, 831 (1985).
[33] Although the previous numerical studies done by Onoda *et al.* (Ref. 25) are about the two-dimensional case, we expect that this phase diagram holds true both in the 2D Z_2 QSH systems and in the 3D Z_2 QSH systems.
[34] R. Shindou *et al.* (unpublished).
[35] D. Vollhardt and P. Wölfle, Phys. Rev. Lett. **45**, 842 (1980); Phys. Rev. B **22**, 4666 (1980).